DOI: 10.26599/FSHW.2025.9250822



Contents lists available at SciOpen

Food Science and Human Wellness

journal homepage: https://www.sciopen.com/journal/2097-0765

China Food Publishing Co.

# Barbaloin from *Aloe vera* alleviates DSS-induced ulcerative colitis by modulating gut microbiota, serum metabolism and MAPK/NF-κB signaling pathway

Zuomin Hu[#1], Zhongxing Chu[#1,2], Qi Wu[1], Feiyan Yang[1], Dandan Qin[3], Yaping Zhou[1], Yiping Tang[1], Feijun Luo[*1,2], Qinlu Lin[1*]

[1]*Hunan Key Laboratory of Deep Processing and Quality Control of Cereals and Oils, State Key Laboratory of Utilization of Woody Oil Resource, Central South University of Forestry and Technology, Changsha, 410004, Hunan, China.*

[2]*Pindingshan Industrial Technology Research Institute, Henan Academy of Sciences, Zhengzhou, 450003, Henan, China.*

[3]*Hunan Institute of Agricultural Product Processing and Quality Safety, Hunan Academy of Agricultural Sciences, Changsha 410125, Hunan, China.*

**ABSTRACT:** Ulcerative colitis (UC) is a multifactorial, chronic inflammatory bowel disease with complex pathogenesis, posing significant challenges for therapeutic intervention. Barbaloin, a bioactive compound derived primarily from *Aloe vera*, exhibits diverse pharmacological properties, including anti-inflammation, anticancer, and organ-protective effects. This study comprehensively evaluated the anti-colitis function of barbaloin through *in vivo* and *in vitro* models. In the DSS-induced mouse colitis model, the administration of barbaloin significantly ameliorated disease severity, as confirmed by the reduced clinical and pathological damage. Notably, barbaloin restored gut microbiota homeostasis and increased beneficial bacterial genera (*Akkermansia*, *Bacteroides*, and *Parabacteroides*), while inhibiting the pathogenic *Escherichia-Shigella*. Serum metabolomics revealed changes in key metabolites such as 9-hpode and PE-NMe2 (22:6/14:1), indicating their involvement in lipid metabolism. Network pharmacology discovered that MAPK and NF-κB signaling pathways were potential targets for the action of barbaloin, and molecular docking and dynamics simulation showed that they had stable binding interactions. *In vitro*, barbaloin suppressed LPS-induced inflammation in RAW264.7 macrophages by inhibiting MAPK/NF-κB activation. Collectively, these findings elucidate a dual mechanism whereby barbaloin ameliorates colitis through microbiota-metabolite reprogramming and suppression of pro-inflammatory signaling, which provides a foundation for its development as a novel UC therapeutic agent.

**KeyWords:** Barbaloin; Ulcerative colitis; Gut microbiota; Serum metabolites; MAPK-NF-κB

## 1. Introduction

Ulcerative colitis (UC) is a chronic inflammatory bowel disease (IBD) of unknown etiology, characterized by continuous mucosal inflammation and ulceration in the colon[1]. The disease manifests clinically with diarrhea, abdominal pain, and rectal bleeding, and in severe cases may progress to colorectal

[#]These authors contributed equally to this work.
***Corresponding author**
Qinlu Lin: linqinlu@hotmail.com;
Feijun Luo: Email: luofeijun@hotmail.com

Received 25 April 2025
Received in revised from 29 May 2025
Accepted 17 July 2025

cancer[2, 3]. While the exact pathogenesis remains unclear, UC is considered to result from complex interactions between genetic predisposition, environmental factors, and gut microbiota dysbiosis[4]. Current treatment strategies focus on pharmacological interventions, including anti-inflammatory drugs, immunosuppressants, and biologics, tailored to disease severity[5, 6]. However, these therapies often have significant side effects that impact patients' quality of life[7, 8]. Emerging evidence suggests dietary modification may play a protective role in UC management. Certain dietary components can modulate gut microbiota composition and attenuate intestinal inflammation, potentially benefiting susceptible individuals[9, 10].

*Aloe vera* has been widely recognized as a valuable health food with a long history of use in traditional Chinese medicine and dietary therapy[11]. *Aloe vera* leaves contain a wealth of anthraquinones, particularly barbaloin (BAR), which has shown significant pharmacological potential. Accumulating evidences indicate that BAR may possess a variety of biological activities, including antitumor, antioxidant, and anti-inflammatory effects[12]. Experimental studies have elucidated BAR's therapeutic mechanisms in inflammatory conditions. In the LPS-induced acute lung injury model, BAR treatment exhibited dose-dependent inhibition of myeloperoxidase (MPO) activity and suppressed phosphorylation of key inflammatory mediators (IκBα and p65)[13]. Furthermore, BAR significantly attenuated the expressions of pro-inflammatory cytokines, including TNF-α and IL-6, suggesting its potential as a protective agent against inflammatory disorders[14]. These findings collectively indicate that BAR's anti-inflammatory effect stems from its modulation of critical inflammatory signaling pathways[15]. In the LPS-induced Caco2 cells, BAR treatment could inhibit LPS-caused the activation of phosphorylation AMPK[16]. In UC animal models, the efficacy of BAR is mainly manifested by repairing intestinal barrier damage[16, 17]. While existing studies support the therapeutic potential of BAR for UC, its precise molecular mechanisms remain to be fully elucidated.

The recent studies showed that gut microbiota and their metabolites might play an important role in nutrient absorption and immune modulation[18, 19]. Adding natural active components to the daily diet is an important way for the regulation of gut microbiota. Meanwhile, the development of IBD was often accompanied by the changes in the microbial composition of the gut, which trigger metabolite changes dominated by bile acid derivatives, short-chain fatty acids and tryptophan metabolites[20]. Such changes in metabolite levels were not only found in intestinal contents but also in the blood and urine. Among these changes, the increase in harmful metabolites and the decrease in beneficial metabolites can directly promote the development of IBD and systemic inflammation. Currently, some food sources have been found to effectively improve the gut microbiota and its metabolites, thereby alleviating UC[21]. BAR, as a dietary active component, has been found to modulate gut microbial composition in a variety of animal models. After 13 weeks of BAR gavaging to rats, the ratio of *Firmicutes*/*Bacteroidetes* in the rat gut was decreased in a concentration-dependent manner[22]. In sepsis mouse model, BAR treatment also promoted the proliferation of

beneficial bacteria (*Lactobacillus* and *Mucispirillum*)[23]. However, the effect of BAR on gut microbiota in UC model is unknown.

In this study, we aimed to evaluate the therapeutic efficacy of BAR on DSS-induced UC, focusing particularly on its ability to alleviate by regulating the gut microbiota and metabolites. Additionally, we sought to explore the impact of BAR treatment on key signaling pathways and target genes in the intestinal tissues of UC mice. This research may provide new insights into the development of alternative strategies for UC.

## 2. Materials and methods

### *2.1 Experimental reagent*

BAR (CAS: 1415-73-2; 95% purity), purchased from Shanghai Yuanzhong Biotechnology Center. DSS (purity≥98%) and LPS were purchased from Sigma-Aldrich (St. Louis, MO, USA). MTS assay purchased from Promega Corporation (Madison, WI, USA). Polyclonal antibody TNF-α (11948), IL-1β (12507), iNOS (13120), IL-6 (12912), β-Actin (12620) and the primary antibodies of ZO-1 (21773-1-AP), Claudin-1 (13050-1-AP) were purchased from Cell Signaling Technology Company (Beverly, MA, USA). Anti-mouse IgG HRP conjugate (W4021) and anti-rabbit IgG HRP conjugate (V7951) were purchased from Promega Corporation (Madison, WL, USA). Fetal bovine serum was bought from Inner Mongolia Opcel Biotechnology Co., Ltd. and Dulbecco's modified essential medium were provided by Gibco-BRL (Carlsbad, CA). All other reagents of this study were the analytical grade.

### *2.2 Animal experiment*

Thirty C57BL/6 male mice (weighing 21-23g, 8 weeks old) were purchased from Hunan Slaike Jingda Laboratory Animal Company (license number: SCXK (Xiang) 2019-0004). Ethics Committee approval number: IACUC-2021(3)068. The mice were acclimated to appropriate temperature and humidity conditions (22-25 ℃, 55-77% humidity) for 6 days before the formal start of the experiment. All mice were fed a standard diet and purified water, and followed a 12-hour light/night cycle. After the adaptation period, the experimental mice were divided into three groups, 10 mice in each group: blank control group (CON); Model group (DSS); BAR protection group (DSS+BAR). The mice were free to drink and eat during the experiment. The mice in the CON group were treated with quoted purified water during the experiment. Based on our preliminary experimental results, we selected 200 mg/kg BAR dose (gavage) evaluating its efficacy against UC (Supplementary Figure 1). The mice in DSS group and DSS+BAR group drank pure water on the first and second days of the experiment, and the normal drinking water of the mice was replaced by 3% (W/V) DSS on the 3th to 14th days of the experiment. In addition, DSS+BAR group mice were treated with 200 mg/kg BAR daily by gavage from day 1 to the end of the experiment. At the same time, the CON and DSS groups were given the same volume of normal saline by gavage to ensure the scientific nature of the experiment.

The mental state and vitality of the mice were monitored throughout the experiment. The disease activity index (DAI) scores of mice in all groups were also evaluated. For details, refer to previous studies[24]. All mice were fasted the day before the end of the experiment. All mice were sacrificed using deep anesthesia with

isoflurane. Mice were dissected as described previously, and organs, blood and intestinal contents were removed and recorded for the experiments.

*2.3 Histopathology analysis*

An appropriate length of distal colon tissue was taken, gently rinsed with pre-cooled phosphate buffered saline (PBS) solution, removed non-tissue material, and completely immersed in tissue fixative solution for more than 24 h. After fixation, paraffin embedding, sectioning, section deparaffinization, and hematoxylin and eosin (H&E) staining were performed. Colonic epithelial cells and tissues were visualized using an Olympus microscope (Olympus Inc., Tokyo, Japan).

*2.4 MPO activity and malondialdehyde (MDA) content measurement*

The appropriate length of the middle segment of colon tissue was accurately weighed and added to 0.9% normal saline at a ratio of 1:9 to prepare 10% homogenate. After centrifugation, the supernatant was removed, and then strictly according to the instructions of the corresponding kit (NanJing JianCheng Bioengineering Com. Nanjing, Jiangsu, China).

*2.5 Western Blot*

The protein of colon tissues or cell samples was extracted with RIPA buffer (containing 1% protease inhibitor, 1% phosphatase inhibitor and 1.0 mmol/L PMSF). This mixed system was incubated on ice for 1 h. The protein concentration was determined by Nanodrop 2000. Subsequently, the resulting protein solution was added to 5 × SDS loading buffer. SDS-PAGE gels (8%-12%) were prepared according to the molecular weight of the proteins. Electrophoresis was stopped after loading until the bands were completely separated. After electrophoresis, the proteins in the gel were transferred to the polyvinylidene fluoride (PVDF) membrane by wet rotation and constant pressure at 60V. After the membrane transfer, the PVDF membrane was put into the blocking solution containing 5% bovine serum albumin. After incubation at room temperature for 2-3h, the PVDF membrane was transferred to the primary antibody corresponding to the target protein, and incubated at 4℃ overnight. The next day, the membranes were washed three times with 1 × Tris Buffered Saline with Tween® 20 (TBST) solution for 5-10 min each time, and then the membranes were put into the corresponding secondary antibody and incubated at room temperature for about 1 h. After that, the membranes were washed three times with 1 × TBST solution for 5-10 min each time. Finally, the bands were obtained in a gel imaging system (ChemiDoc XRS+, BIO-RAD) by dropping the developer onto the PVDF membrane and exposing it.

*2.6 RT-qPCR*

Total RNA was extracted by adding TransZol-Up (TransGen Biotech Co., Ltd, Beijing, China). RNA quality and concentration were analyzed, and RNA integrity was checked. Single-stranded cDNA was synthesized using 1.2 μg of total RNA and HiScript IV RT SuperMix for qPCR (Vazyme Biotech Co., Ltd, Nanjing, Jiangsu, China). RT-qPCR was performed using a real-time quantitative PCR system (CFX96, Applied Biosystems Co., Ltd, Waltham, MA, USA). The reaction program was set as follows: prechange to

94℃ for 3 min; Denaturation was performed at 94℃ for 30 s. Annealing at 60 ℃ for 40 s; The extension was carried out at 72 ℃ for 1 min with a cycle number of 40. The 2−ΔΔCt (RQ) method was used to calculate the relative expression of target genes. The primer sequences were shown in Table 1.

**Table 1** Primers for PCR assay list

| Gene | Forward primer | Reverse primer |
|---|---|---|
| β-actin | 5'-CCA TAA ACG ATG CCG GA-3' | 5'-CAC CAC CCA TAG AAT CAA GA-3' |
| Il-6 | 5'-ATG GAT GCT ACC AAA CTG GAT-3' | 5'-TGA AGG ACT CTG GCT TTG TCT-3' |
| Il-1β | 5'-GAG CAC CTT CTT TTC CTT CAT CTT-3' | 5'-TCA CAC ACC AGC AGG TTA TCA TC-3' |
| Tnf-α | 5'-CAA AAT TCG AGT GAC AAG CCT G-3' | 5'-GAG ATC CAT GCC GTT GGC-3' |
| inos | 5'-CAG CTG GGC TGT ACA AAC CTT-3' | 5'-CAT TGG AAG TGA AGC GTT TCG-3' |
| Cox-2 | 5'-ATG CTC CTG CTT GAG TAT GT-3' | 5'-CAC TAC ATC CTG ACC CAC TT-3' |

*2.7 DNA sequencing and gut microbiota analysis*

Genomic DNA was extracted from cecal contents using a rapid DNA spin extraction kit according to the manufacturer's instructions. DNA purity and quality were detected and analyzed. Primers 338F (5'-ACTCCTACGGGAGGCAGCA-3') and 806R (5'-GGACTACHVGGGTWTCTAAT-3') were used to amplify the V3-V4 region of the 16S rRNA gene. The amplified products were identified, extracted and further purified. Purified amplicons were quantitatively sequenced on an Illumina MiSeq platform using QuantiFluor™-ST (Promega, USA) according to standard protocols (Majorbio Corporation, Shanghai, China). The results were analyzed.

*2.8 Determination of serum metabolites by using untargeted metabolomics*

According to the requirements for sample preparation, 100 μL serum samples (n = 6 per group) were collected for serum metabolomics analysis. The metabolome profile was measured using a UHPLC-QTOF-MS system (AB Sciex Pte. Ltd, Milford, MA, USA). Raw data were analyzed using Progensis QI software (Waters Co., Milford, MA, USA). Progensis QI was used to identify metabolites. The structure of metabolites was analyzed using human metabolome database (HMDB) and metlin. The MajorBio Cloud Platform was then used to analyze and process the data. In addition, Spearman correlation analysis was used to evaluate the correlation between the differences in gut bacteria in each group and the composition of variable metabolites.

*2.9 Network pharmacological prediction*

Through swisstargetprediction (http://www.swisstargetprediction.ch/) collection of BAR target protein. In disgent database (https://www.disgenet.org/) input "Inflammation", search, target proteins related diseases. Using Venny2.1 (https://bioinfogp.cnb.csic.es/) map interactions both targets, according to the results of overlap target genes is the BAR potential targets for the treatment of inflammation. The potential targets were imported into the STRING database (https://cn.string-db.org/) and processed to export the core target interaction map in the form of TSV. The specific processing method was referred to the previous article. Cytoscape 3.9.1 software was used to process and analyze the interaction maps. The DAVID database was imported into the potential core targets of BAR in the treatment of inflammation, and after setting up

appropriate processing and analysis conditions, GO BP, GO CC, GO MF, and KEGG enrichment analysis were performed. The final result of using microscopic letter (http://www.bioinformatics.com.cn/) output.

*2.10 Molecular docking and molecular dynamics simulations*

A semi-flexible docking method was used to study the interaction between complex receptors and ligands. The receptor protein was processed using Schrodinger software, excess water molecules were removed and polar hydrogen atoms were added, and the protein receptor point charge was calculated. The structure of the ligand small molecule was drawn using 2D Sketcher and processed to meet the docking requirements. The docking procedure was performed using SP docking. The specific procedures and parameters were referred to previous study[25, 26].

To further investigate the complex interaction between the receptor and ligand and its stability, molecular dynamics (MD) simulation was performed. The protein-ligand complex was simulated for 100ns using GROMACS2020.6. The AMBER99SB-ILDN force field was selected to construct the protein topology file, and the Amber 20.0 and GAFF force fields were used to generate the small molecule ligand topology file. After balancing the system charges, different methods were used to reduce the energy of the complex. At suitable temperatures, the complexes were subjected to NVT integration simulations and NPT equilibrium simulations. Specific procedures and parameters were referred to previous studies[25, 26].

*2.11 Cell culture*

Murine mononuclear-macrophage leukemia cells RAW264.7 were obtained from Xiangya Medical College. BAR was dissolved in dimethylsulfoxide (DMSO). Cells in the logarithmic growth phase were selected, the cell concentration was adjusted to $5 \times 10^4$, and the cells were seeded in 96-well plates. When cells were cultured until adherent, different concentrations BAR were added into the plates for 24 h. Micrographs of each well were taken using an inverted microscope (DMI3000B, Lecia Microsystems CMS GmbH, Germany). MTS were added to plates after images were obtained and this incubated at 37°C for 30 min. Using microplate reader (Thermo Multiskan SPECTRUM Thermo Fisher Scientific, Waltham, MA, USA) to measure the absorbance at 490 nm.

*2.12 Luciferase reporter activity*

The luciferase reporter gene vector containing the NF-κB binding sequence was transfected into the cells, and the cells were lysed after a certain time after cell treatment and the luciferase was extracted. Finally, the fluorescence intensity was measured using a luciferase assay system to reflect the activity of NF-κB.

*2.13 Statistical analysis*

All experiments were performed at least three parallel experiments, and the data were normalized to the control level by the control group. All data were analyzed with the use of SPSS 13.0 software (SPSS, Chicago, Illinois). All experimental data were expressed as mean ± standard deviation. Data that conformed to a normal distribution were performed one-way analysis of variance (ANOVA) test analysis. If the distribution of data did not conform to normality, the nonparametric Kruskal-Wallis test was used to analyze the differences

among groups with a two-tailed test. $P < 0.05$ was considered statistically significant, $P < 0.01$ was considered extremely significant, $P < 0.001$ was considered abnormally significant.

## 3. Results

### *3.1 The effect of BAR on the phenotype of UC mice*

The time schedule for the experimental period is shown in Figure 1A. The results showed that the mice in the DSS group had obvious hematochezia and diarrhea (Figure 1B). BAR treatment alleviated DSS-induced hematochezia and diarrhea. Weight loss is one of the important indicators to measure the success of DSS-induced UC model in mice. The body weight of the mice in the CON group increased by 11.35% compared with the initial body weight. The growth rate of mice in the DSS group showed a downward trend from the seventh day, and the body weight of mice in the DSS group was significantly different from that in the CON group from the 11th day ($P < 0.01$). Mice in the DSS group showed significant weight loss at the later stage, indicating that the DSS-induced UC model was successfully established. BAR treatment slowed down DSS-induced weight loss and had highly significant differences (Figure 1C). DAI score is used to assess the degree of UC in mice. The feces of the mice in the DSS group were thinner after the mice drank DSS water freely. In the later stage of the experiment, the DSS-induced mice appeared diarrhea, hematochezia, and reduced activity. These symptoms were alleviated with BAR treatment (Figure 1D). Spleen is an important lymphoid immune organ in the body. Its size and shape reflect the immune level of the body. The spleen size of the mice was significantly different among the three groups (Figure 1E). Compared with the CON group, the spleen index of the DSS group increased by 1.75 times ($P < 0.01$). Compared with the DSS group, the spleen of the DSS+BAR group was significantly smaller and the spleen index was decreased by 8.93% ($P < 0.05$). These results indicated that the BAR treatment could improve the symptoms of DSS-induced UC in mice.

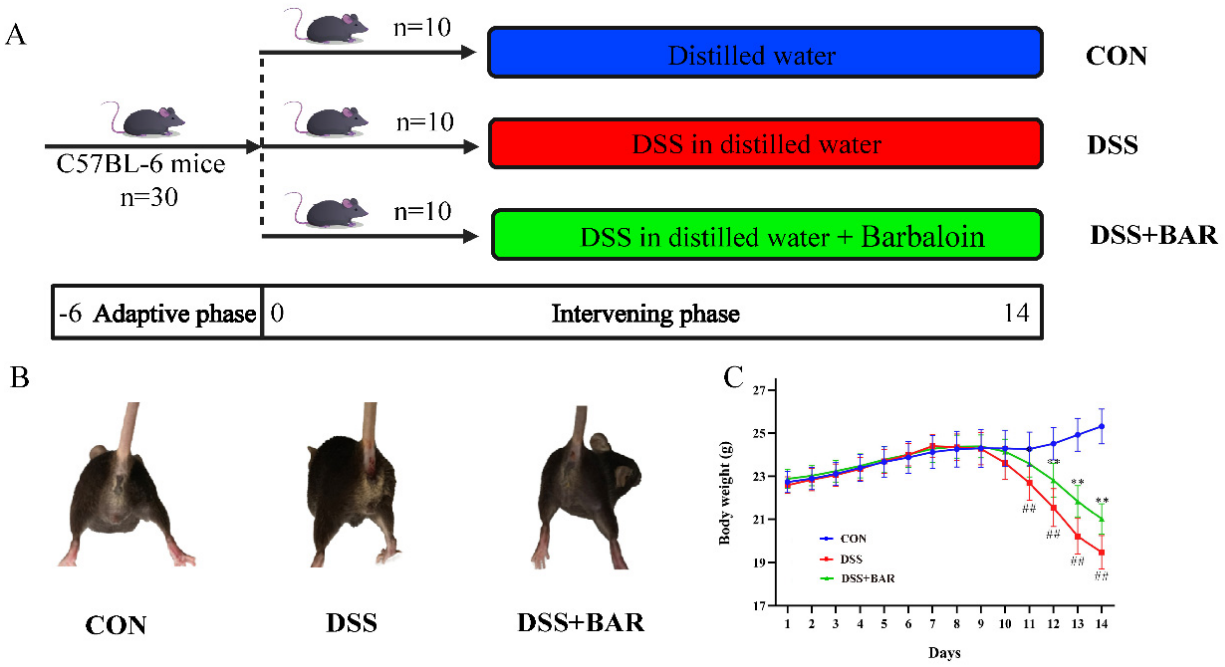

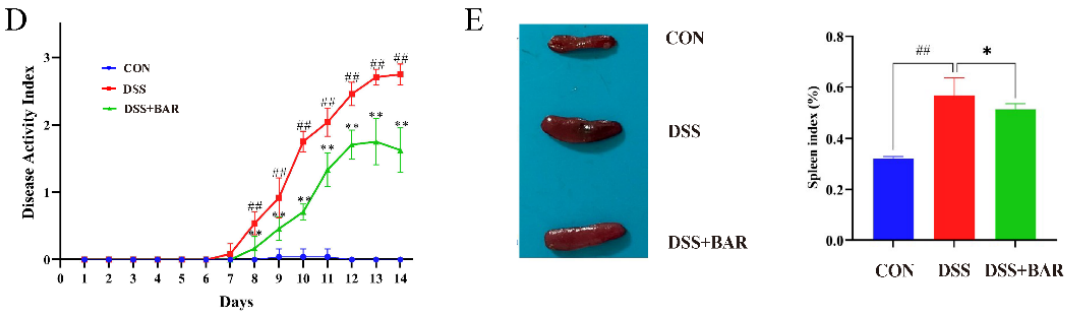


**Fig.1.** The effect of BAR on phenotype of UC mice. (A) Animal treatments schedule; (B) Rectal bleeding in mice; (C) Changes in body weight of mice; (D) Changes in DAI scores; (E) Changes of spleen and its index in mice. CON: Control group; DSS: DSS group; DSS+BAR: DSS+200 mg/kg BAR group. DAI: Disease activity index. Data are presented as means ± SEM, n = 10. #: $P < 0.05$; ##: $P < 0.01$ vs CON group; *: $P < 0.05$; **: $P < 0.01$ vs DSS group.

### *3.2 The effect of BAR on the UC mice colon*

After the mice were sacrificed, the colon of mice was observed and measured (Figure 2A). The results showed significant differences in the changes of colon length among the three groups. The length of colon in DSS group was shortened to 0.80 times of that in CON group ($P < 0.01$). This change in colon length might be caused by edema. the colorectal length in the DSS+BAR group was increased by 9.57% compared with the DSS group ($P < 0.05$). The extent of colonic injury in the mice was analyzed with H&E staining (Figure 2C). Compared with the CON group, the crypt structure of colon glands in the DSS group was destroyed. Goblet cells were also significantly reduced, and a large number of inflammatory cells infiltrated. The structure of mucosa and crypt in the DSS+BAR group was relatively intact. There was no obvious inflammatory cell infiltration, indicating that BAR might protect the colonic mucosal barrier and reduce inflammatory injury.

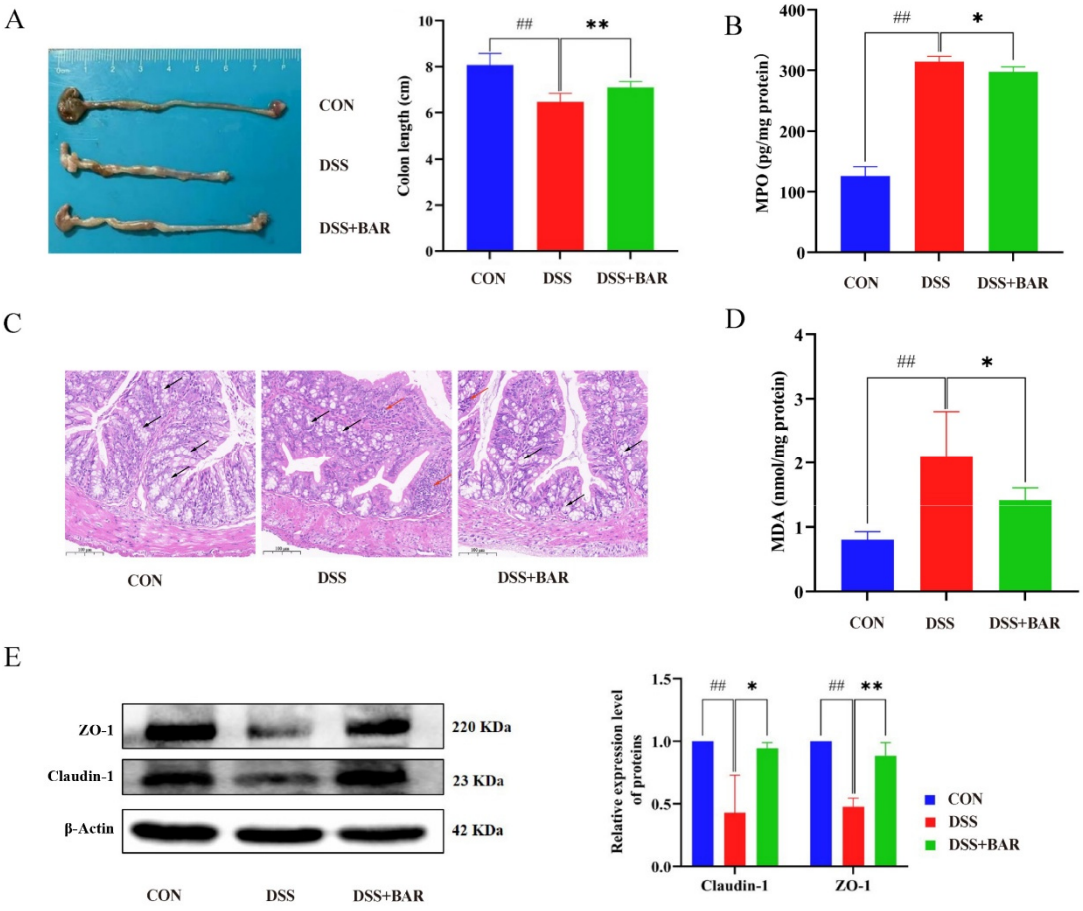

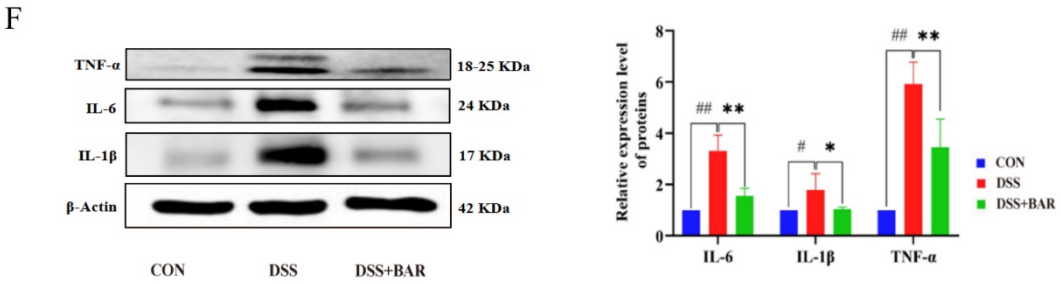


**Fig.2.** The effect of BAR on colonic phenotype of UC mice. (A) Changes in colon length in mice; (B) MPO changes in colon tissue of mice; (C) Pathological section of mouse colon. Black arrows indicated representative goblet cells and red arrows indicated representative inflammatory infiltration; (D) Changes of MDA in colon tissue of mice; (E) Changes of colon tissue barrier protein expression in mice. (F) The effect of BAR on the protein expression of inflammatory factors. CON: Control group; DSS: DSS group; DSS+BAR: DSS+200 mg/kg BAR group. MPO: Myeloperoxidase; MDA: Malondialdehyde. Data are presented as means ± SEM, n = 10. #: $P < 0.05$; ##: $P < 0.01$ vs CON group; *: $P < 0.05$; **: $P < 0.01$ vs DSS group.

MPO activity is often used as one of the indicators to evaluate the severity of UC. Compared with the CON group, MPO activity in the colon tissue of the DSS group was increased by 2.50 times ($P < 0.01$). After BAR treatment, MPO activity was significantly decreased, which decreased by 5.40% compared with DSS group ($P < 0.05$) (Figure 2B). MDA content is also often used as an indicator to evaluate the severity of UC. Compared with the CON group, MDA content in the colon tissue of the DSS-treated group increased by 2.60 times ($P < 0.01$). After BAR treatment, MDA content was significantly decreased by 32.86% compared with the DSS group ($P < 0.05$) (Figure 2D). These results suggest that BAR can alleviate colonic tissue injury by reducing the activation and infiltration of granulocytes and oxidative stress.

The intestinal barrier is the main defense line of the body against intestinal bacteria and antigens, and DSS stimulation can damage the intestinal barrier. We explored the effect of BAR on the intestinal barrier of UC mice at the protein level (Figure 2E). Compared with the CON group, the relative protein expression values of ZO-1 and Claudin-1 in the DSS group decreased to 0.48 and 0.43 times, respectively. Compared with the DSS group, the DSS+BAR group increased by 83.33% and 118.60%, respectively. It suggests that BAR is beneficial to alleviate the damage of intestinal barrier induced by DSS stimulation.

IL-1β, IL-6 and TNF-α are widely studied cytokines with pro-inflammatory effects, and their abnormal expression is closely related to the severity of inflammation. Compared with the CON group, the relative protein expression levels of IL-1β, IL-6 and TNF-α in the colon tissue of the DSS group were increased by 1.79 times ($P < 0.01$), 3.31 times ($P < 0.05$) and 5.92 times ($P < 0.01$), respectively. Compared with the DSS group, the expression of three inflammatory factors in the BAR protection group decreased by 13.4%, 68.58% and 41.72%, respectively (Figure 2F). These results indicate that BAR treatment can effectively reduce the high expression of inflammatory factors induced by DSS in colon tissue, thereby preventing UC.

*3.3 BAR alleviated the dysbiosis of gut microbiota in UC mice*

The dilution curve of the sobs diversity index indicated that the sequencing volume was sufficient and that this test met the requirements (Figure 3A). The rank-abundance curve showed that there were species differences between the CON group, DSS group and DSS+BAR group (Figure 3B). By evaluating the Chao index and Shannon index, we found that the DSS treatment significantly reduced the abundance of gut microbiota. BAR treatment appeared to reduce the disruption of gut microbiota abundance by DSS, but this

improvement was not significantly different (Figure 3C/D). Principal coordinate analysis (PCoA) showed that there were significant differences among the three groups of samples in OTU levels ($p$ = 0.001) (Figure 3E). The CON group was furthest away from the DSS group, while the DSS+BAR group was closer to the CON group. This suggests that the gut microbiota of BAR-treated UC mice is recovering to normal levels.

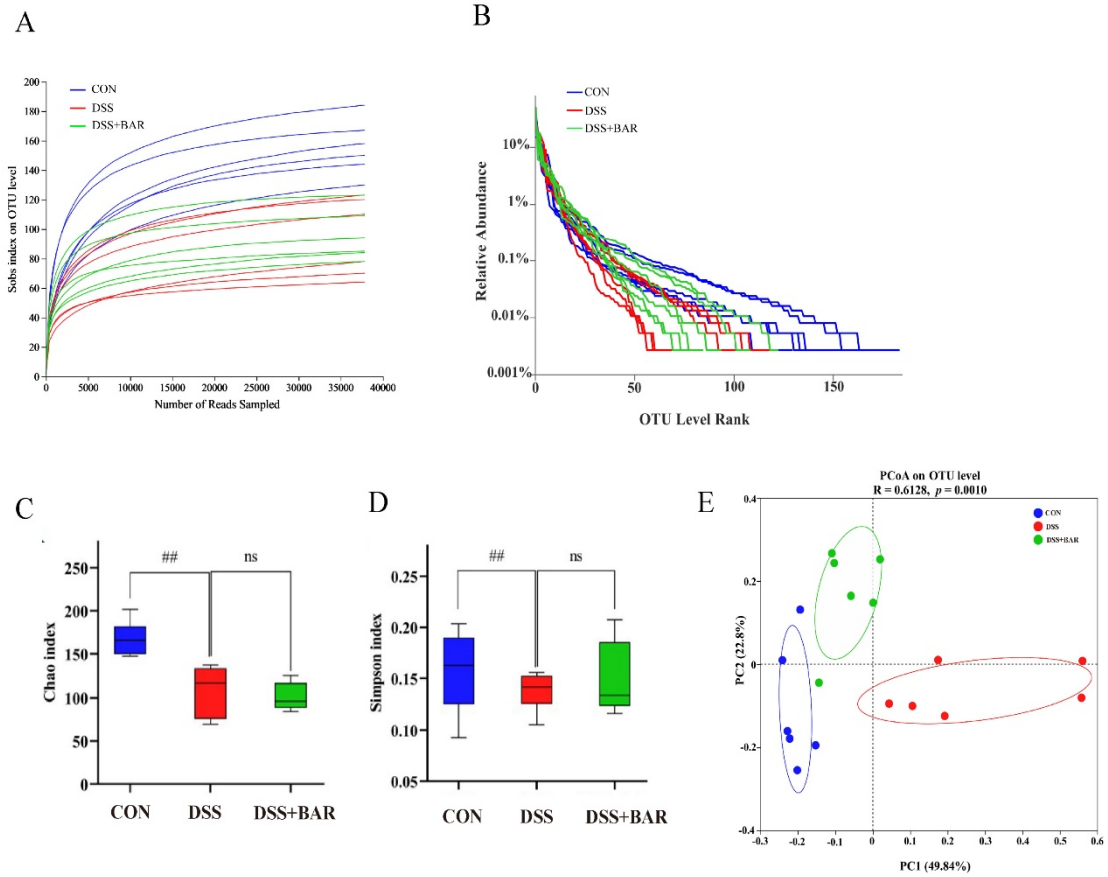


**Fig.3.** Basic information and diversity of gut microbiota data (A) Sobs index dilution curve; (B) Rank-abundance curve; (C) Chao index; (D) Simpsion index; (E) Principal coordinate PCoA analysis. CON: Control group; DSS: DSS group; DSS+BAR: DSS+200 mg/kg BAR group. OTU: Operational taxonomic unit; PCoA: Principal coordinate analysis. Data are presented as means ± SEM, n = 6. #: $P < 0.05$; ##: $P < 0.01$ vs CON group; *: $P < 0.05$; **: $P < 0.01$ vs DSS group.

At phylum level, the results showed that DSS stimulation significantly reduced the relative abundance of *Firmicutes*, *Verrucomicrobiota* and *Deferribacterota* compared with the CON group (Figure 4A). And the multiples were 0.47 times ($P < 0.01$), 0.50 times ($P > 0.05$) and 0.34 times ($P < 0.05$) of CON group, respectively. The relative abundance of *Firmicutes*, *Verrucomicrobiota* and *Deferribacterota* increased by 53.90% ($P < 0.01$), 221.49% ($P < 0.01$) and 77.89% ($P < 0.01$) in DSS+BAR group compared with DSS group. Compared with the CON group, DSS stimulation significantly increased the relative abundance of *Bacteroidetes* and *Proteobacteria* by 12.79 times ($P < 0.01$) and 80.00 times ($P < 0.01$), respectively. Compared with DSS group, the relative abundance of *Bacteroidetes* and *Proteobacteria* in BAR treatment group decreased by 77.89% ($P < 0.01$) and 83.00% ($P < 0.01$), respectively (Figure 4B-E). The ratio of *Firmicutes* to *Bacteroidetes* in the CON, DSS, and DSS+BAR groups was 26.24 ± 6.76, 0.95 ± 0.24, and 6.58 ± 1.78, respectively (Figure 4G). BAR treatment significantly restored DSS-induced changes in the ratio of *Firmicutes* to *Bacteroidetes*. At the genus level, *Akkermansia*, *Lactobacillus*, *Faecalibaculum*, *Allobaculum*, *Bacteroides*, *Parabacteroides*, *Erysipelatoclostridium*, *Escheria-Shigella*, *norank_f_Muribaculaceae* and

*Enterococcus* were the dominant species in 3 groups (Figure 5A). To study the differences bacteria, the Kruskal-Wallis H test was used to analyze the top 15 bacteria of genus-level abundance (Supplementary Figure 2A). The results showed that *Akkermansia*, *Bacteroides*, *Escheria-Shigella*, *Parabacteroides*, *Parasutterella*, *Colidextribacter* and *norank_f_Lachnospiraceae* might be bacteria that undergo significant changes after BAR treatment. Among them, the abundance of *Akkermansia*, *Bacteroides*, *Escheria-Shigella* and *Parabacteroides* had significant changes. Compared to DSS group, *Akkermansia*, *Bacteroides*, *Escheria-Shigella* and *Parabacteroides* were extremely significantly ($P < 0.01$) affected by BAR treatment (Figure 5B-E). The abundance of *Bacteroides*, *Escheria-Shigella* and *Parabacteroides* in DSS group was significantly higher than that in CON group by 58.48, 1983.75 and 293.4 times, respectively ($P < 0.01$). In DSS+BAR group, the abundance of *Bacteroides*, *Escheria-Shigella* and *Parabacteroides* were significantly lower than those in DSS group by 72.09%, 81.79% and 95.30%, respectively ($P < 0.01$). *Akkermansia* was significantly decreased after DSS treatment. BAR treatment could significantly increase its abundance, which was 221.49% higher than DSS group ($P < 0.01$). The abundance of *Parasutterella*, *Colidextribacter* and *norank_f_Lachnospiraceae* was shown in Supplementary Figure 2B-D. These results suggest that BAR may play an important role in regulating the composition of the gut microbiota.

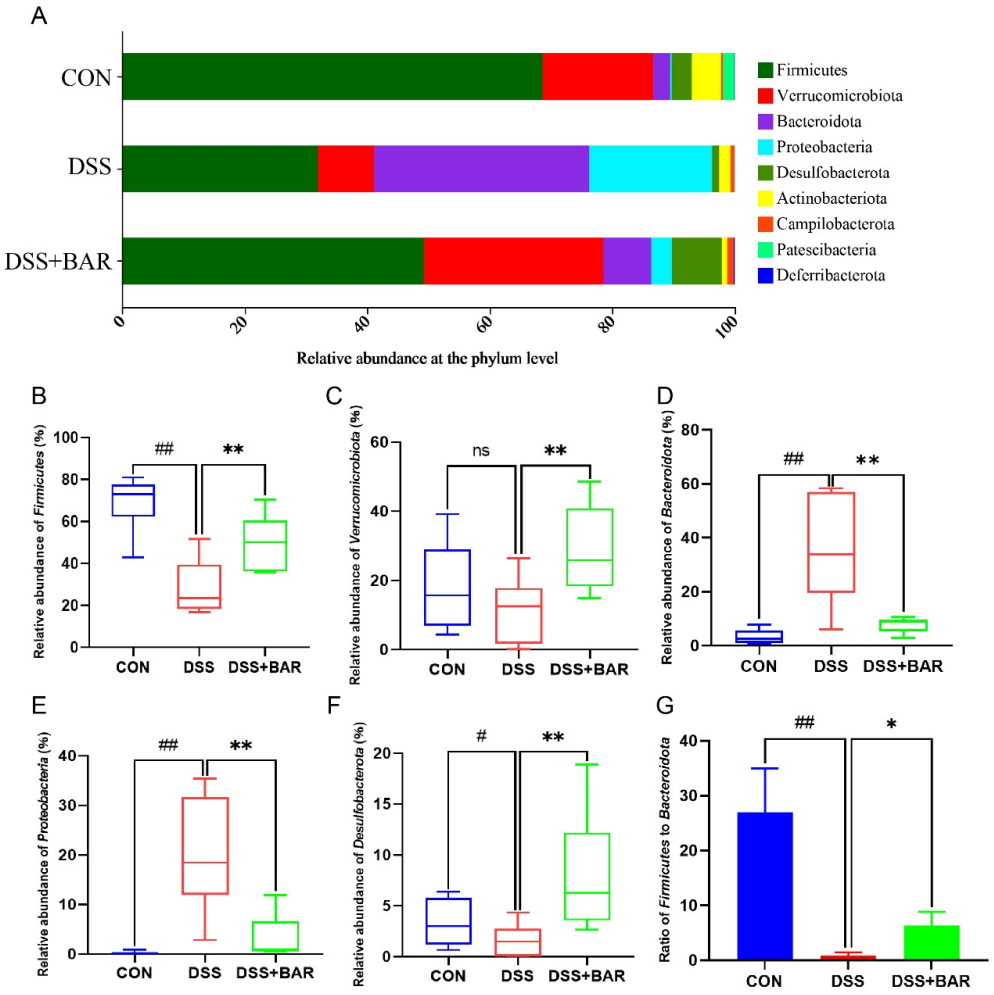


**Fig.4.** Analysis of community composition at the phylum level. (A) The percentage of community abundance at phylum level; (B-F) Richness changes of the flora at the phylum level; (G) Ratio of Firmicutes to Bacteroidetes. CON: Control group; DSS: DSS group; DSS+BAR: DSS+200 mg/kg BAR group. Data are presented as means ± SEM, n = 6. #: $P < 0.05$; ##: $P < 0.01$ vs CON group; *: $P < 0.05$; **: $P < 0.01$ vs DSS group.

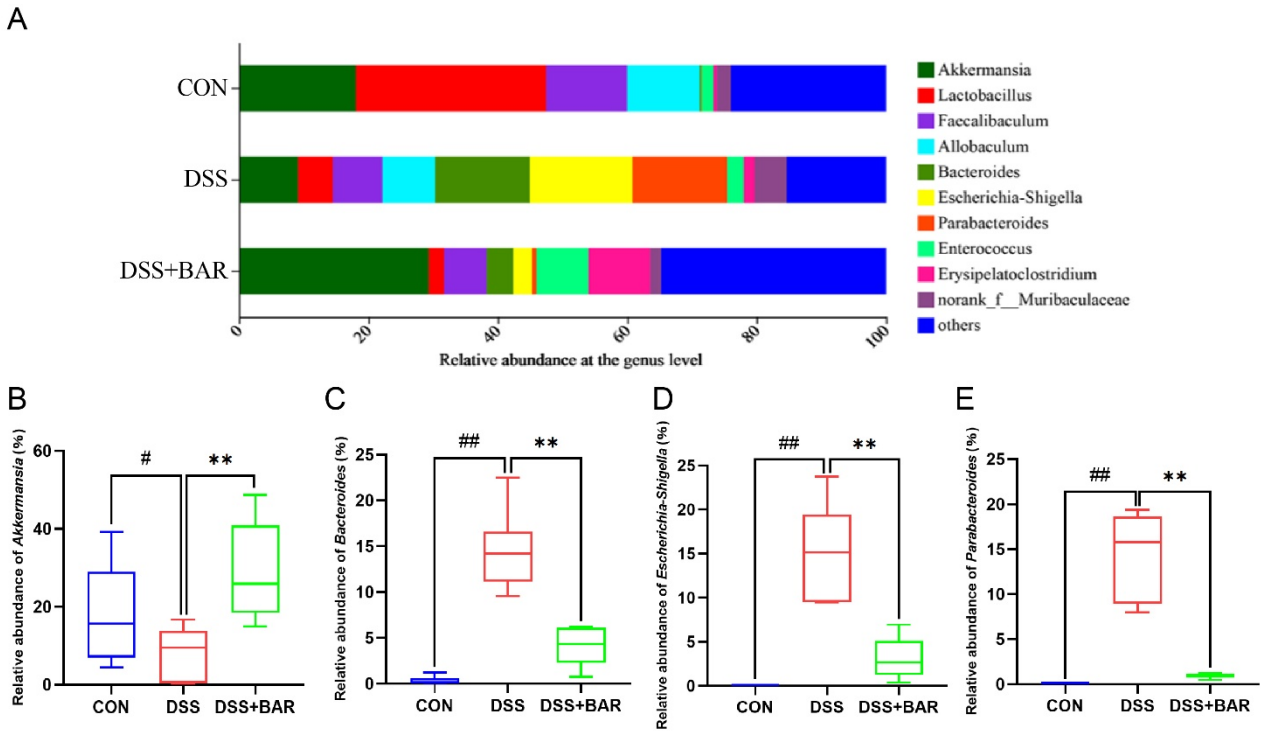


**Fig.5.** Analysis of community composition at the genus level. (A) The percentage of community abundance at genus level; (B-E) Richness changes of the flora at the genus level. Data are presented as means ± SEM, n = 6. #: $P < 0.05$; ##: $P < 0.01$ vs CON group; *: $P < 0.05$; **: $P < 0.01$ vs DSS group.

### *3.4 BAR improved the serum metabolism in UC mice*

Serum metabolites were examined and these were categorized into 18 groups according to Human Metabolome Database (HMDB). Among them, lipids and lipid molecules (36.98%), organic acids and their derivatives (18.46%) and organic heterocyclic compounds (14.70%) were main substances (Figure 6A). Partial least squares-discriminant analysis (PLS-DA) was performed for the different treatment groups. The different treatment groups demonstrated a good degree of separation in positive and negative ion mode (Figure 6B/C). We defined metabolites with variable importance in projection (VIP) value > 1 and $p$ value < 0.05 as differential metabolites. Compared with the CON group, 151 metabolites were significantly decreased and 430 metabolites were significantly increased in the DSS group (Figure 6D). Compared with the DSS group, 97 metabolites were down-regulated and 75 metabolites were up-regulated in the DSS+BAR group (Figure 6E). Metabolic analysis revealed that the metabolites regulated by BAR included 109 kinds, of which 48 metabolites belonged to lipids and lipid molecules; 33 metabolites belonged to organic acids and their derivatives; 28 metabolites belonged to heterocyclic organic compounds (Supplementary Figure 3A). KEGG enrichment analysis of these differential metabolites show that BAR treatment affect mainly the metabolism of linoleic acid, glycerophospholipid metabolism, and the biosynthesis of phenylalanine, alanine and tryptophan (Supplementary Figure 3B). These results suggest that BAR treatment primarily affects lipid metabolism in the blood.

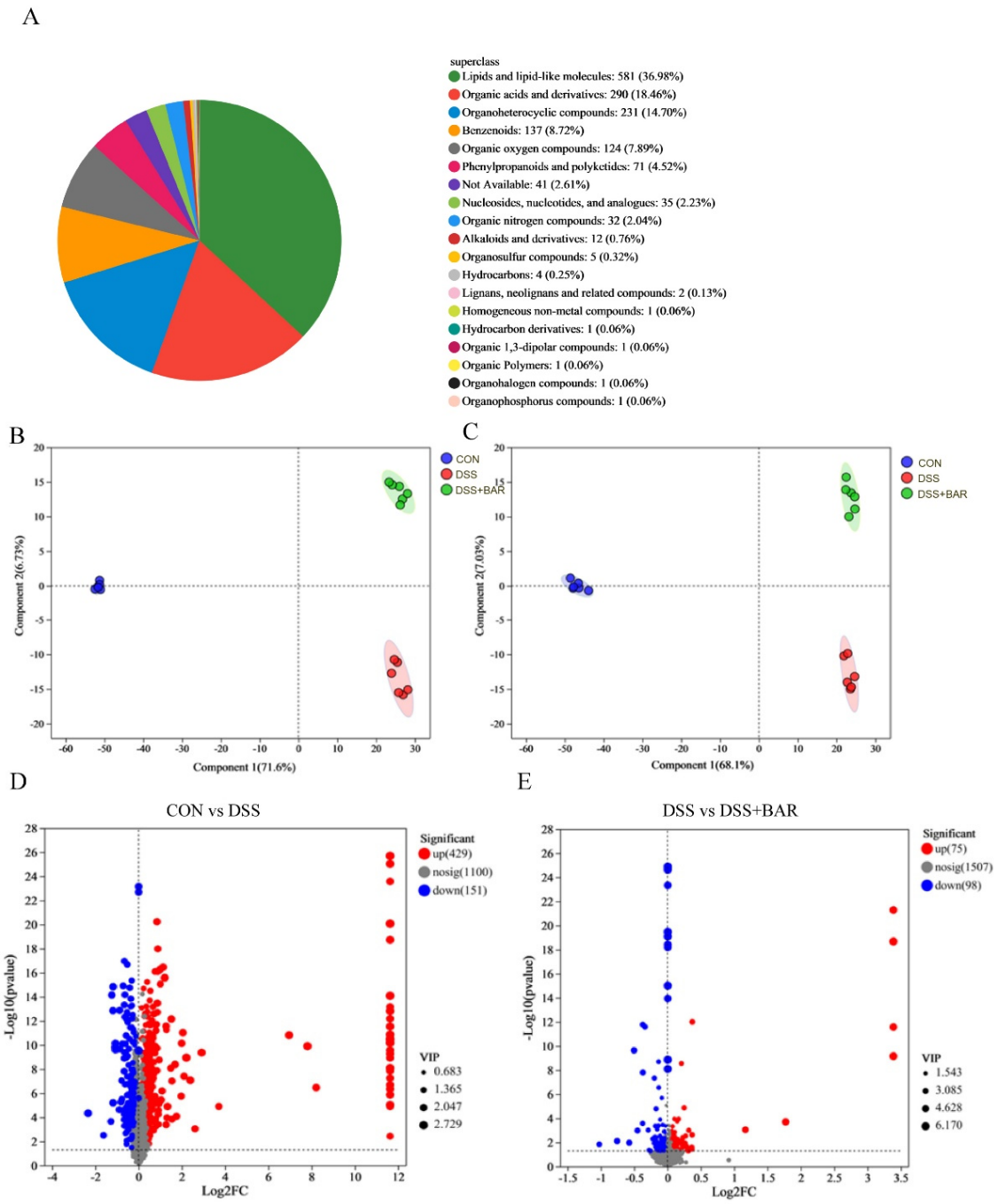


**Fig.6.** Analysis of serum metabolic samples. (A) Classification of metabolites in HMDB; (B-C) PLS-DA score plot of mouse serum samples in positive and negative ion mode; (D-E) Volcano plot of differential metabolites. CON: Control group; DSS: DSS group; DSS+BAR: DSS+200 mg/kg BAR group; HMDB: Human Metabolome Database; PLS-DA: Partial least squares-discriminant analysis; VIP: Variable importance in projection.

Venn diagram showed that BAR treatment restored the down-regulation of 20 metabolites in the CON group due to DSS stimulation; BAR treatment restored the up-regulation of 18 metabolites in the CON group due to DSS stimulation (Figure 7A). The cluster heat map was used to show the relative abundance of 38 differential metabolites in different treatment groups (Figure 7B). KEGG pathway enrichment analysis was performed with the differential metabolites (Figure 7C). This result showed that BAR might regulate linoleic acid metabolism, glycerophospholipid metabolism and arachidonic acid metabolism to alleviate the symptoms of UC in mice.

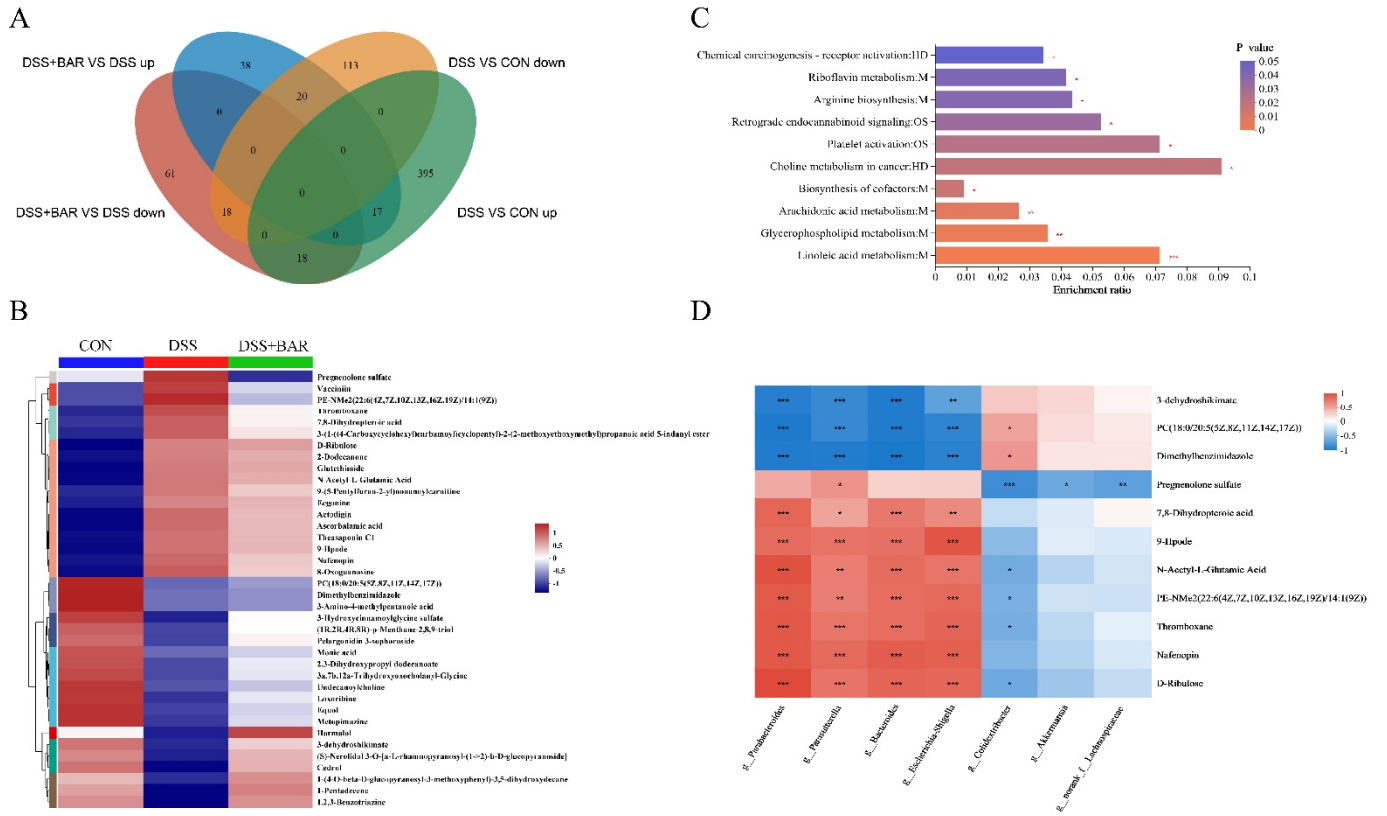


**Fig.7.** Analysis of differential metabolites in serum. (A) Venn diagram of significantly different metabolites; (B) heat map of differential metabolites; (C) KEGG pathway enrichment analysis; (D) Spearman's correlation analysis between gut bacteria and differential serum metabolite. CON: Control group; DSS: DSS group; DSS+BAR: DSS+200 mg/kg BAR group. KEGG: Kyoto encyclopedia of genes and genomes. *: $P < 0.05$, **: $P < 0.01$, ***: $P < 0.001$.

### *3.5 Relationship between gut microbiota and serum metabolites in UC mice*

We used Spearman's correlation analysis to explore potential relationships between gut microbiota (genus level) and serum metabolites (Figure 7D). The result showed that *Parabacteroides*, *Parasutterella*, *Bacteroides, Escherichia-Shigella* and *Colidextribacter* were significantly associated with serum metabolite changes. *Akkermanisa* and *norank_f_Lachnospiraceae* were significantly associated with pregnenolone sulfate. *Parabacteroides*, *Parasutterella*, *Bacteroides, Escherichia-Shigella* were positively correlated with pregnenolone sulfate, 7, 8-dihydropteroic acid, 9-hpode, N-acetyl-L-glutamic acid, PE-NMe2(22:6(4Z,7Z,10Z,13Z,16Z,19Z)/14:1(9Z)), thromboxane, nafenopin and D-ribulose; *Parabacteroides*, *Parasutterella*, *Bacteroides, Escherichia-Shigella* were negatively correlated with 3-dehydroshikimate, PC (18:0/20:5(5Z,8Z,11Z,14Z,17Z)), dimethylbenzimidazole. The correlation between *Colidextribacter*, *Akkermanisa*, *norank_f_Lachnospiraceae* and these metabolites were reversed. The results suggest that BAR may be able to ameliorate the severity of ulcerative colonic inflammation in mice by modulating the gut microbiota to improve serum metabolites.

### *3.7 Pharmacological analysis of BAR network*

In addition to gut microbiota and serum metabolites, the molecular mechanisms by which BAR directly affected colitis are not clear. We used network pharmacology to explore potential targets for BAR intervention in colitis. Venn diagram was generated by data collation and analysis to identify 18 potential targets of BAR with anti-inflammatory effects (Figure 8A). Referring to previous studies, PPI node maps were generated after

the score value was set to > 0.4, and 18 protein interaction maps were generated (Figure 8B). After enrichment and visualization of this result, it was evident that the top five core targets were MAPK1, NF-κB, TNF, IL-6, and IL-1β (Figure 8C). GO analysis mainly included biological process (BP), cellular component (CC) and molecular function (MF). The top ten of BP, CC and MF were analyzed (Figure 8D). Results showed that BAR may play a role in the positive regulation of interleukin-6 production, inflammatory response and cellular response lipopolysaccharide, DNA−binding transcription activator activity, RNA polymerase II-specific, RNA polymerase II-specific DNA-binding transcription factor binding and other processes. In addition, the 20 most significant ($P$ < 0.05) KEGG pathways were selected for demonstration and study (Figure 8E). These signaling pathways include a variety of disease signaling pathways, such as IBD, NF-κB signaling pathway, Toll-like receptor signaling pathway, MAPK signaling pathway. In summary, based on network pharmacology analysis, BAR may mainly regulate the inflammatory response of the body through MAPK and NF-κB pathways.

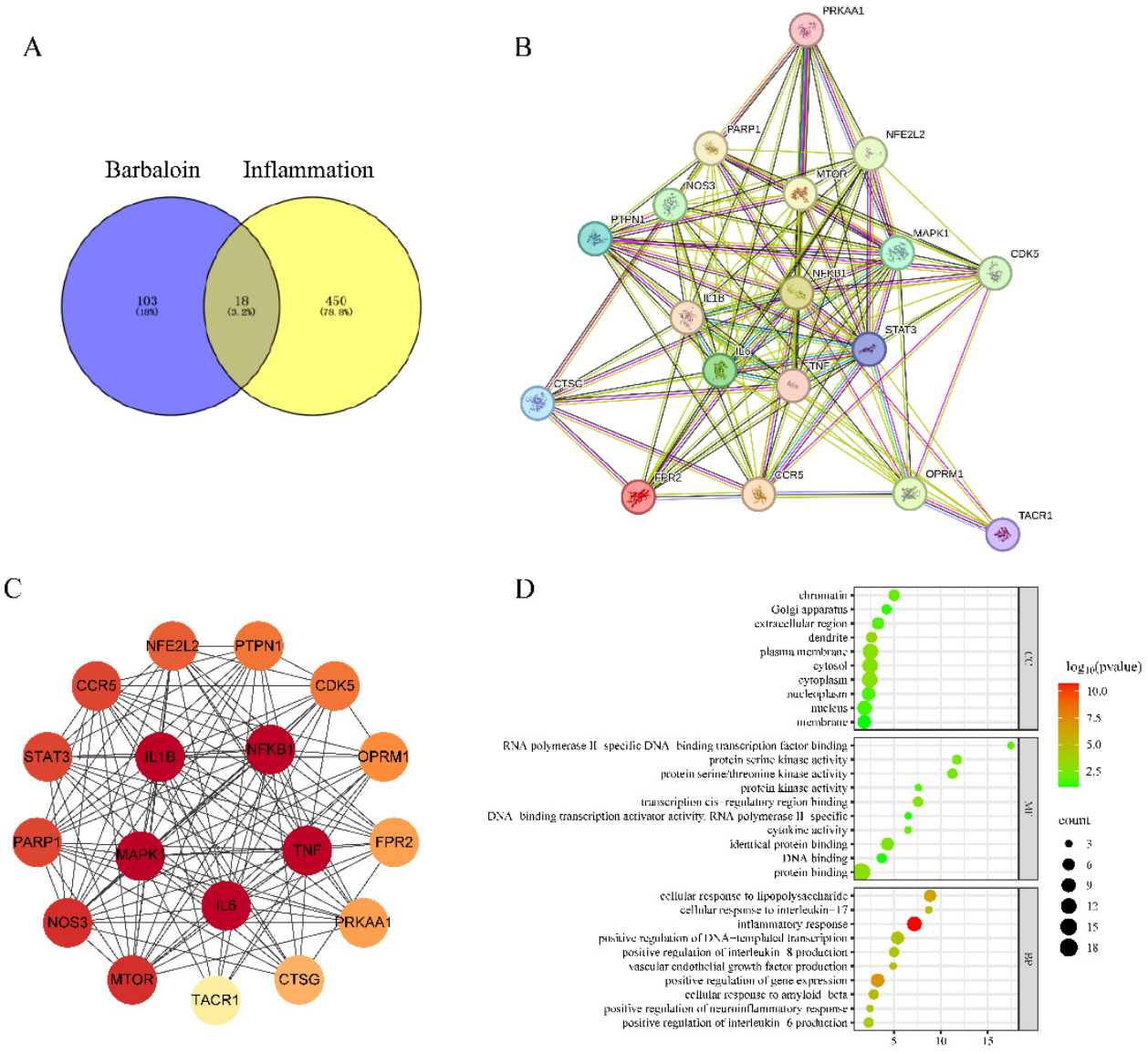

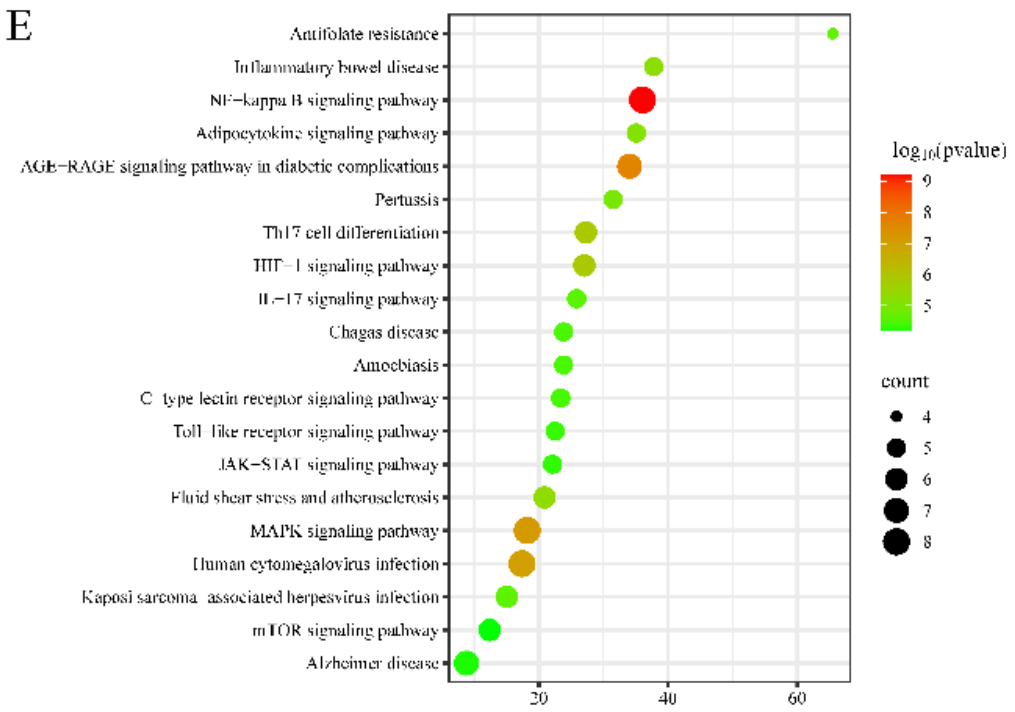


**Fig.8.** Screening and enrichment analysis of potential anti-inflammatory targets of BAR. (A) Venn diagram of BAR and inflammatory targets; (B) PPI map among core targets; (C) Grading map of core targets; (D) GO analysis; (E) KEGG pathway enrichment analysis. PPI: Protein-protein interaction networks; GO: Gene ontology; KEGG: Kyoto encyclopedia of genes and genomes.

### *3.8 Molecular docking and molecular dynamics simulation analysis between BAR and core targets*

Molecular docking can identify the interactions between molecules and predict the receptor-ligand binding mode and complex structure. BAR was subjected to standard precision molecular docking with p38 MAPK and NF-κB (Figure 9). The binding energies of the two receptor proteins and BAR were -4.959 and -4.609 kcal/mol, respectively. From previous studies, the negative binding energy indicates that BAR can bind to two different receptor proteins and that they have strong binding between them. This also suggested that BAR had the potential to regulate the NF-κB/MAPK signaling pathway. Based on the molecular docking results, the ability of BAR to act on the core targets was further verified.

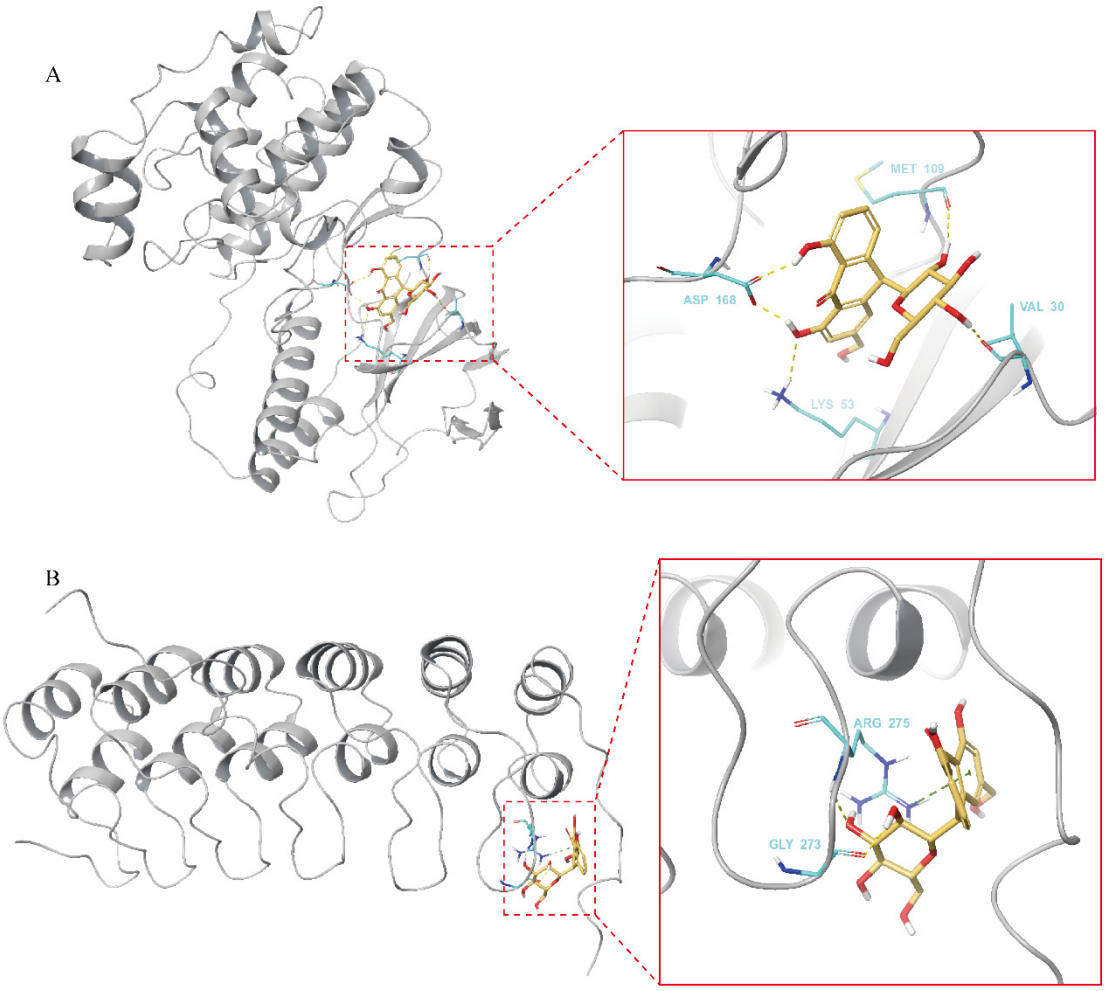


**Fig.9.** The Molecular docking of BAR with p38 MAPK (A)and NF-κB (B).

Molecular dynamics simulation can help to study the dynamic stability of receptor-ligand complexes. Based on the binding force of the complex and the ligand-receptor interaction, MD simulations of BAR and core target protein receptors were performed. Root mean square deviation (RMSD) is used as a metric to quantify the average displacement of a particular atom in a particular frame compared to a reference frame. The analysis of RMSD can indicate whether an equilibrium is reached during the simulation. The figure shows that the RMSD curve of BAR and the two ligands forming a complex eventually converges in a stable range. Especially after p38 MPAK and BAR were combined, RMSD tended to a stable value, indicating that the protein-ligand complex was in equilibrium (Figure 10A/C). BAR can maintain a stable equilibrium state after binding to two different target proteins, which is of great significance for regulating the biological functions of the target proteins. Root mean square fluctuation (RMSF) is a quantitative method to evaluate the stability of amino acid residues in proteins by measuring their fluctuation levels during simulation. This index serves as an indicator of the sturdy rigidity and dynamic stability of the protein. Higher RMSF values at the beginning and end of the curve indicate higher amino acid freedom of the protein, residues in contact with the ligand are marked in green, and most amino acids have low values due to contact or persistent interaction with the ligand (Figure 10B/D). Ligands can reduce the degrees of freedom of amino acids in the target protein, thereby enhancing protein stability. After binding to BAR, different target proteins can maintain structural stability in a dynamically changing environment, showing excellent adaptability and stability.

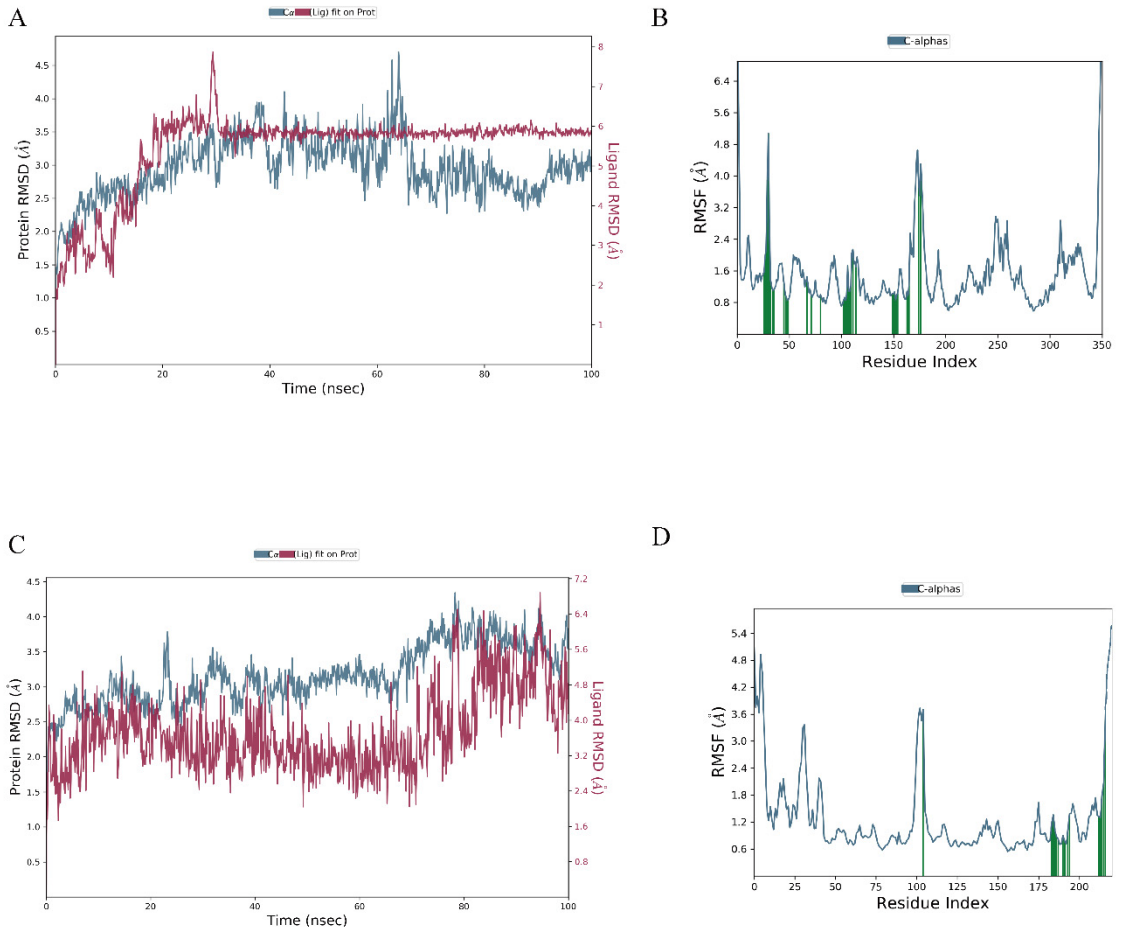


**Fig.10.** Molecular dynamics simulations of BAR and p38 MAPK and NF-κB. (A) RMSD values of BAR and p38 MAPK complexes; (B) RMSF of BAR and p38 MAPK complexes; (C) RMSD values of BAR and NF-κB complexes; (D) RMSF of BAR and NF-κB complexes. RMSD: Root mean square deviation; RMSF: Root mean square fluctuation.

### *3.9 Effects of BAR on downstream targets of NF-κB/MAPK signaling pathway*

Combined with the network pharmacology analysis, we speculated that BAR might affect the activity of NF-κB/MAPK signaling pathway to inhibit inflammatory response. In serum metabolomics analysis, changes in these serum metabolites might be associated with arachidonic acid metabolism. This was also potentially related to the NF-κB/MAPK signaling pathway. To test the direct link between BAR and the NF-κB/MAPK signaling pathway, we used Western Blot to analyze the expressions of NF-κB/MAPK-related proteins in mouse colon tissues (Figure 11). The results showed that the relative protein expression levels of phosphorylated p38 and ERK1/2 in the DSS group were 2.39 ± 0.60 and 2.83 ± 0.71, respectively. In DSS+BAR group, they were 1.52 ± 0.38 and 1.62 ± 0.41. Compared with the DSS group, the relative protein expression of p-p38 and ERK1/2 in the DSS+BAR group decreased to 0.64 times ($P < 0.05$) and 0.57 times ($P < 0.05$). The results showed that BAR inhibited the phosphorylation of p38 and ERK1/2 in the MAPK pathway. This demonstrated the ability of BAR to directly target p38 MAPK. Since NF-κB was a key upstream target of MAPK, the direct effect of BAR on MAPK signaling might be related to its regulation of NF-κB.

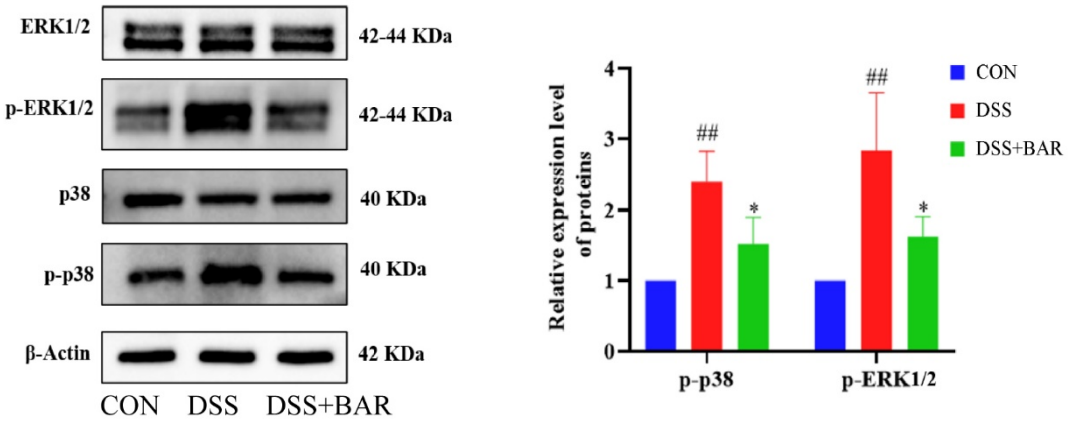


**Fig.11.** Effect of BAR on the phosphorylation of p38 and EKR1/2 proteins in the colon. CON: Control group; DSS: DSS group; DSS+BAR: DSS+200 mg/kg BAR group. Data are presented as means ± SEM, n = 6. #: $P < 0.05$; ##: $P < 0.01$ vs CON group; *: $P < 0.05$; **: $P < 0.01$ vs DSS group.

### *3.10 Effect of BAR on LPS-induced RAW 264.7*

To determine the anti-inflammatory properties of BAR *in vitro*, the LPS-induced RAW264.7 macrophage inflammation model was used in the present study. It was clarified that BAR was not toxic to RAW264.7 cells at different concentrations. In addition, the cell activity of the solvent group and the cell activity of different concentrations of BAR treatment were not significantly different from that of the CON group ($P > 0.05$). This indicated that BAR did not significantly affect the activity of RAW246.7 cells in the concentration range of 100 μg/mL (Figure 12A/B). After the addition of LPS, both RT-qPCR (Figure 12C) and Western Blot (Figure 12D/E) results showed that LPS successfully induced inflammatory factor accumulation in RAW264.7 cells. BAR treatment inhibited this changes in inflammatory factors at the mRNA and protein levels. The protein expressions of IL-6, IL-1β, TNF-α, COX-2 and iNOS in the maximum concentration 100 μg/mL BAR treatment group were significantly lower than those in the DSS group by 54.35%, 47.84%, 74.03%, 55.60% and 79.65%, respectively. This indicated that BAR could reduce the inflammatory response by down-regulating the protein expression levels of IL-6, IL-1β, TNF-α, COX-2 and iNOS. This ability of BAR to inhibit the expression of inflammatory factors might be related to its inhibition of NF-κB transcriptional activity. Reported gene results showed that compared with LPS group, the relative luciferase activity of NF-κB in 25 μg/mL, 50 μg/mL and 100 μg/mL BAR treatment groups decreased by 33.90%, 44.25% and 56.90%, respectively (Figure 12F). The effect of BAR on phosphorylated proteins ERK1/2, p38, and JNK in the MAPK signaling pathway was explored at the protein level (Figure 12G/H). Compared with the CON group, the phosphorylation levels of ERK1/2, p38 and JNK were significantly upregulated in the LPS group, indicating that LPS-induced inflammation activated ERK1/2, p38 and JNK in the MAPK signaling pathway. Compared with the LPS group, the low concentration of BAR (25 μg/mL) had no significant effect on the phosphorylation levels of p38, ERK1/2 and JNK proteins. But the 50 μg/mL and 100 μg/mL of BAR treatment significantly inhibited the phosphorylation levels of p38, ERK1/2 and JNK proteins. Compared with the LPS group, the relative protein expressions of phosphorylated p38, ERK1/2 and JNK in 100 μg/mL BAR treatment group were decreased by 32.84%, 62.14% and 50.00%, respectively ($P <$

0.01). These results suggested that BAR exerted anti-inflammatory effects through regulating the phosphorylation level of MAPK and the activity of NF-κB transcription factor, as well as the expression levels of its downstream genes and proteins, which further verified our previous experimental results.

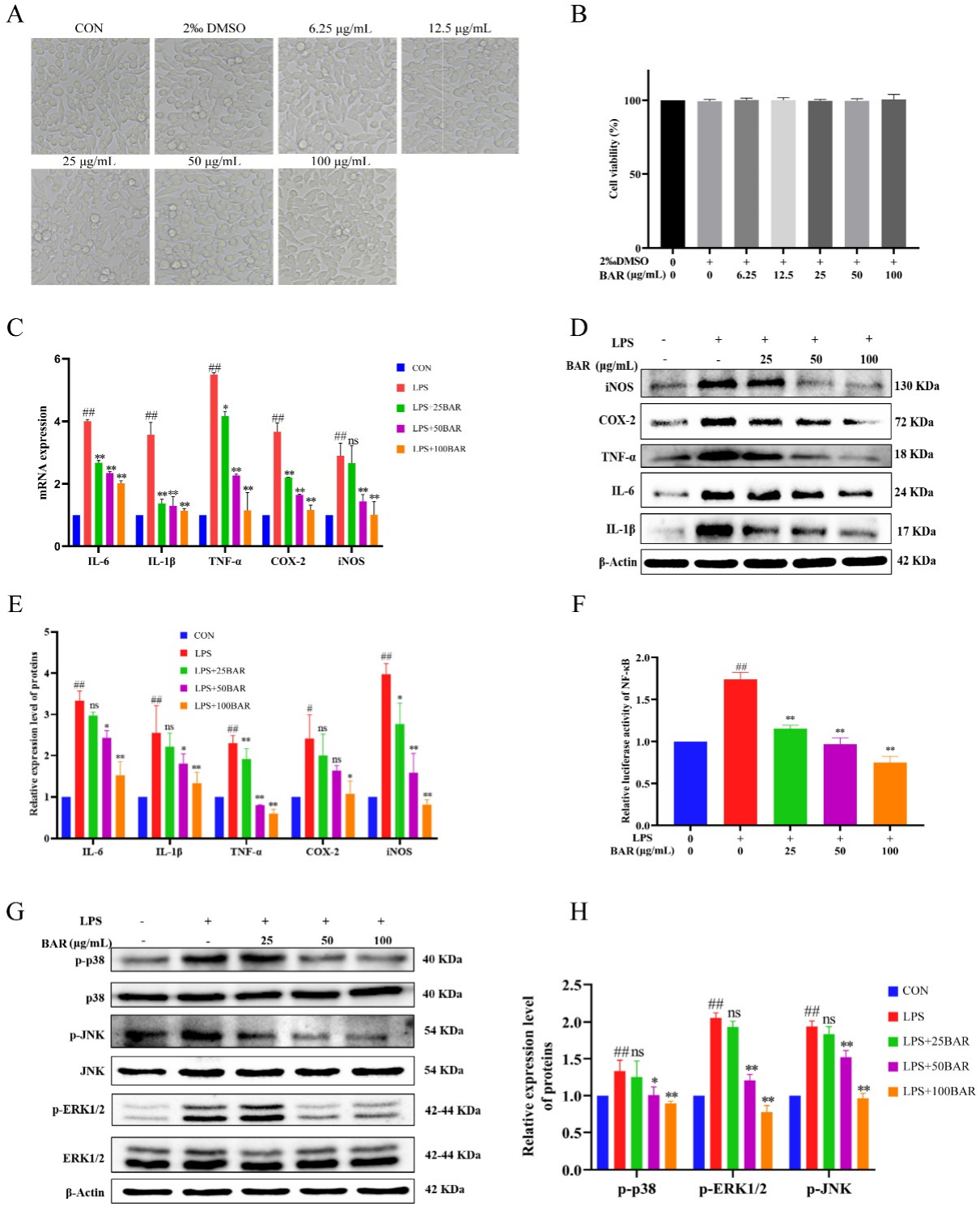


**Fig.12.** The anti-inflammatory effect of BAR was verified *in vitro*. The effect of BAR on RAW246.7 cell (A) morphology and (B) activity; (C) The effect of BAR on mRNA expression of inflammatory factors in LPS-induced RAW246.7 cells; (D-E) The effect of BAR on protein expression of inflammatory factors in LPS-induced RAW246.7 cells; (F) The effect of BAR on the transcriptional activity of NF-κB in LPS-induced RAW246.7 cells; (G-H) The effect of BAR on the MAPK signaling pathway in LPS-induced RAW246.7 cells; Data are presented as means ± SEM, n = 6. #: $P < 0.05$; ##: $P < 0.01$ vs CON group; *: $P < 0.05$; **: $P < 0.01$ vs LPS group.

## 4. Discussions

BAR has emerged as a highly bioactive food component that has attracted considerable research focus owing to its multifaceted functional properties[19]. BAR exhibits a broad spectrum of organoprotective effects, including hepatoprotection, bone density maintenance, antibacterial activity, kidney protection, blood-brain barrier integrity, blood sugar control[17,28-30]. BAR treatment not only significantly ameliorated body weight loss and the disease activity index (DAI) score but also obviously improved the pathological changes of conic tissues in UC mice, confirming its preventative effect on UC. The spleen, as an important lymphoid organ responsible for immune surveillance, showed a decreased weight after BAR, suggesting that the systemic immune response was regulated[31].

In this study, BAR administration significantly ameliorated DSS-induced UC symptoms, including characteristic weight loss, rectal bleeding and colon shortening. The therapeutic effects of BAR were supported by the evidences: (1) significant amelioration of colonic inflammation, (2) alleviation histopathological damage to colonic tissues, (3) restoration of the integrity of the intestinal barrier. Notably, BAR treatment induced significant alterations in the intestinalota ecosystem, shifting both microbial diversity and abundance. Metabolomics analyses reveal significant changes in the serum metabolites, which may be mechanistically linked to BARs-inflammatory effects by regulating key inflammatory signaling pathways.

Existing evidence indicates that the pathogenesis of UC is closely associated with oxidative stress imbalance. The excessive production of reactive oxygen species (ROS) leads to cellular oxidative stress and molecular damage[32]. This redox imbalance triggers lipid peroxidation, compromises intestinal mucosal barrier integrity, and exacerbates inflammatory responses[33]. Notably, BAR treatment effectively suppressed MPO activity-a neutrophil-derived enzyme whose elevated levels correlate with inflammatory states and oxidative stress[34]. In this study, BAR attenuated DSS-induced the expressions of TNF-α, IL-6, and IL-1β in colon tissues, suggesting that BAR reduces inflammatory response via decreasing the expressions of inflammatory cytokines.

Mechanistically, BAR preserved intestinal barrier function by maintaining tight junction proteins[35]. The damage of intestinal barrier can increase intestinal permeability, further aggravating intestinal inflammation[36, 37]. In the DSS-induced colitis model, BAR can up-regulate the expressions of tight junction proteins (ZO-1, Claudins, and Occludin) of intestinal epithelial cells, which can reduce intestinal permeability and inhibit the entry of bacteria and LPS into the blood, which helps to reduce the inflammatory response of colonic tissues.

The gut microbiota plays a pivotal role in regulating host immune responses, metabolic processes, and developmental pathways, while also influencing the onset and progression of various diseases[38]. There is increasing evidence that the composition of the intestinal microbiota plays a crucial role in the pathogenesis of ulcerative colitis, with specific bacteria exert either pro-inflammatory or anti-inflammatory effects that influence intestinal inflammatory responses[39,40]. In experimental models, DSS-induced colitis is characterized by gut microbiota dysbiosis, marked by reduced probiotic abundance and increased pathogenic

bacterial populations[41, 42]. Our findings corroborate these observations, demonstrating that DSS treatment significantly diminished gut microbial diversity in mice. Although BAR intervention did not significantly alter α-diversity, it induced substantial alterations in the microbial community composition and structure.

At the phylum level, *Firmicutes* and *Bacteroidetes* represent two dominant bacterial groups in the gastrointestinal tract, with their relative abundance serving as a critical biomarker of intestinal homeostasis[43]. This alteration in the ratio of *Firmicutes* and *Bacteroidetes* is associated with intestinal microenvironment imbalance. Among them, the increased level of *Firmicutes* was associated with metabolic disorders, while the increased level of *Bacteroidetes* was associated with IBD[44]. Notably, a clinical study reported that increased *Firmicutes* abundance was observed following fecal microbiota transplantation in UC patients[45]. It suggests the protective role of *Firmicutes* in gut health. Conversely, *Proteobacteria* (a phylum encompassing multiple pathogens, e.g., *Escherichia coli*, *Salmonella*, *Vibrio cholerae*, and *Helicobacter pylori*) are recognized as microbial dysbiosis markers when elevated[46]. The gut microbiota of UC patients frequently exhibit *Proteobacteria* enrichment[47]. This trend in gut microbiota changes was replicated in DSS-induced mice[48]. DSS administration significantly reduced *Firmicutes* abundance while increasing *Bacteroidetes* and *Proteobacteria* proportions. BAR treatment effectively counteracted these dysbiosis-related alterations. Beyond these phylum-level alterations, BAR also restored diminished *Verrucomicrobiota* and *Desulfobacterota* populations, further underscoring its regulatory role in intestinal homeostasis. At the genus level, *Akkermansia* (the sole known gut-resident genus within *Verrucomicrobiota*) showed the reduced abundance in DSS-treated mice, aligning with observations in IBD and metabolic disorder patients[49]. *Akkermansia* contributes to mucosal integrity by enhancing tight junction protein expression and modulating adaptive immunity[50]. BAR intervention reversed DSS-induced depletion of *Akkermansia* and also attenuated the colitis-associated proliferation of commensal *Bacteroides*. This was consistent with previous reports on their environment-dependent role in intestinal inflammation.

The role of gut microbiota and their metabolites in regulating inflammation is not limited to the gut, but extends to the metabolic homeostasis of the host[20]. Our study identified the dysfunction of metabolic homeostasis in DSS-induced UC. The results showed that the endogenous metabolites in UC mice were abnormally changed, and the lipid metabolism-related linoleic acid metabolism, glycerophospholipid metabolism, arachidonic acid metabolism pathways were impaired. Lipids play a crucial role in energy reserve and metabolic supply within the organism. Excessive oxidized lipids in the gut may induce damage to the intestinal epithelial tissue[51]. A number of studies have reported that lipid metabolism was impaired in UC patients, which was further confirmed by IBD animal models. In the linoleic acid metabolic pathway, 9-HpODE is a product of the peroxidation of linoleic acid and is also regarded as one of the biomarkers of oxidative stress *in vivo*[52]. In this study, BAR was found to down-regulate 9-HpODE. Arachidonic acid is a polyunsaturated fatty acid found mainly in the form of phospholipids in cell membranes. Under cellular stress conditions, phospholipase A2 and phospholipase C release arachidonic acid as free arachidonic acid from phospholipids. The arachidonic acid metabolic pathway is subsequently activated by many enzymes and

inflammatory mediators, leading to systemic inflammation in the host[53]. Arachidonic acid can be metabolized to theomboxanel through the cyclooxygenase pathway. Theomboxanel is a prothrombotic, chemically unstable prostaglandin compound that has been shown to promote inflammatory responses in UC[54]. In this study, BAR was found to significantly down-regulate thromboxane.

Metabolites of the gut microbiota traverse through the intestinal barrier and enter the blood, thereby influencing circulating metabolite profiles[55]. These serum metabolites play a crucial role in modulating proinflammatory cytokine expression and can impact intestinal inflammatory responses via systemic pathways[56]. Notably, specific serum metabolites have the potential to be biomarkers of gut health. Consequently, monitoring these metabolites can provide insights into host gut health. Therefore, the current study conducted a correlation analysis of the composition of the gut microbiota and the serum metabolomics profile in the DSS-induced mice. *Paracteroides*, *Parutterella*, *Bacteroides*, *Escherichia-Shigella* were negatively correlated with PC(18:0/20:55Z,8Z,1Z,14Z,17Z)). At the same time, it was positively correlated with 9-hpode, thromboxane and PE-NMe2. The present study was mainly conducted to find the relationship between harmful bacteria and pro-inflammatory lipid mediators. In contrast, beneficial genera such as *Akkermanisa*, *Colidextribacter*, *norank_f_Lachnospiraceae* did not showe significant correlations with these inflammatory metabolites. It suggests that the modulation of inflammatory responses mediated by the gut microbiota may involve the biosynthesis of specific bioactive metabolites. Given the complexity and diversity of the intestinal microbiota ecosystem, its impact on inflammation may involve multiple bacterial species and metabolic pathways[57]. However, further verification is needed by using fecal microbiota transplantation and antibiotic depletion of gut microbiota. In particular, it is to determine the correlation between intestinal microbial metabolites and metabolites in the serum, and to identify which metabolites can also regulate the MAPK/NF-κB signaling, thereby inhibiting the expressions of inflammatory factor genes. Only after this series of research work is completed can we have a chance to know the full picture of the molecular mechanism of BAR in inhibiting colitis. It should be noted that this study was conducted in a mouse model, so whether the results apply to humans still need further verification.

Under adverse external stimuli, the body will activate a variety of immune cells to play an automatic defense function and secrete various inflammatory mediators[58]. This process underpins the pathogenesis of inflammation. RAW246.7 is a commonly used cell model in inflammation research. *In vitro*, it can better demonstrate the characteristics of immune cells[59]. LPS can activate the RAW246.7 internal signaling pathway through the receptor on the cell membrane[60]. This allowed the expression of specific genes and induced the secretion of inflammatory cytokines or chemokines. As a major member of the pathogen-associated molecular pattern, LPS causes cytotoxic inflammatory responses mainly through producing ROS and NO[61]. We chosed LPS-induced RAW264.7 as an inflammation model *in vitro* and determined that BAR did not affect the cell activity of RAW264.7. MAPK signaling pathway is important to regulate the expression of a variety of inflammatory factors[62]. The most central regulatory genes in the MAPK cascade are p38, ERK1/2 and JNK. These kinases are activated by upstream signaling pathways to

produce responses, thereby affecting the activity of downstream transcription factors and up-regulating the expression of inflammatory factors[63]. Among them, p38 is involved in the production of COX-2 and other inflammation-related substances[64]. When inflammation occurs, p38 phosphorylation levels in lesional tissue increase significantly. JNK can induce the phosphorylation of c-Jun N-terminal residues and activate it to nuclear transfer, thereby regulating inflammatory factors and participating in inflammatory response[65, 66]. In colitis, the phosphorylation of ERK leads to functional impairment of the colonic mucosa and reduces intestinal water/sodium absorption[67]. *In vitro*, we demonstrated that BAR treatment improved DSS-induced activation of MAPK signaling in gut tissues. The relationship between NF-κB and inflammation has been an important research direction. Study have shown that MAPKs can activate NF-κB and regulate the expression of inflammatory cytokines[68]. In the D-galactose-induced mice, BAR treatment could improve D-galactose-induced oxidative stress, cognitive dysfunction and inflammation by mediating MAPK and NF-κB signaling pathways[69]. In this study, BAR demonstrated significant inhibition of LPS-induced MAPK pathway activation, as indicated by decreased phosphorylation of p38, JNK, and ERK1/2 ($P < 0.01$). Concurrently, BAR suppressed NF-κB transcriptional activity by 58%, leading to concomitant downregulation of pro-inflammatory mediators at both mRNA and protein levels (qPCR and Western Blot validation). These mechanistic findings were further corroborated *in vivo* through immunohistochemical and ELISA analyses.

## 5. Conclusion

The present study demonstrated that BAR significantly prevented DSS-induced colitis in mice. BAR effectively alleviated UC by inhibiting inflammatory factors, reducing oxidative stress damage, and improving intestinal barrier function. Combined analysis of gut microbiota and serum metabolism indicated that BAR could ameliorate UC through regulation of gut microbiota and associated metabolites in mice. *In vitro*, the experiments showed that BAR inhibited phosphorylation of the MAPK cascade and reduced transcriptional activity of NF-κB, leading to decreased expression of inflammatory factors in immune cells. The potential mechanism of BAR alleviating colitis is shown in Figure 13. These findings provide a theoretical basis for further development of *Aloe vera* as a functional food ingredient and enhance the utilization potential of BAR. For human dietary applications, these results may guide scientifically sound nutritional strategies. However, several unresolved issues remain: The safety profile and dose-response relationship of BAR require clarification. Additional studies focusing on targeted metabolomics of short-chain fatty acids in gut contents are needed to better understand the relationship between gut microbiota-derived metabolites and UC. Addressing these questions will significantly advance the practical applications of *Aloe vera* and BAR.

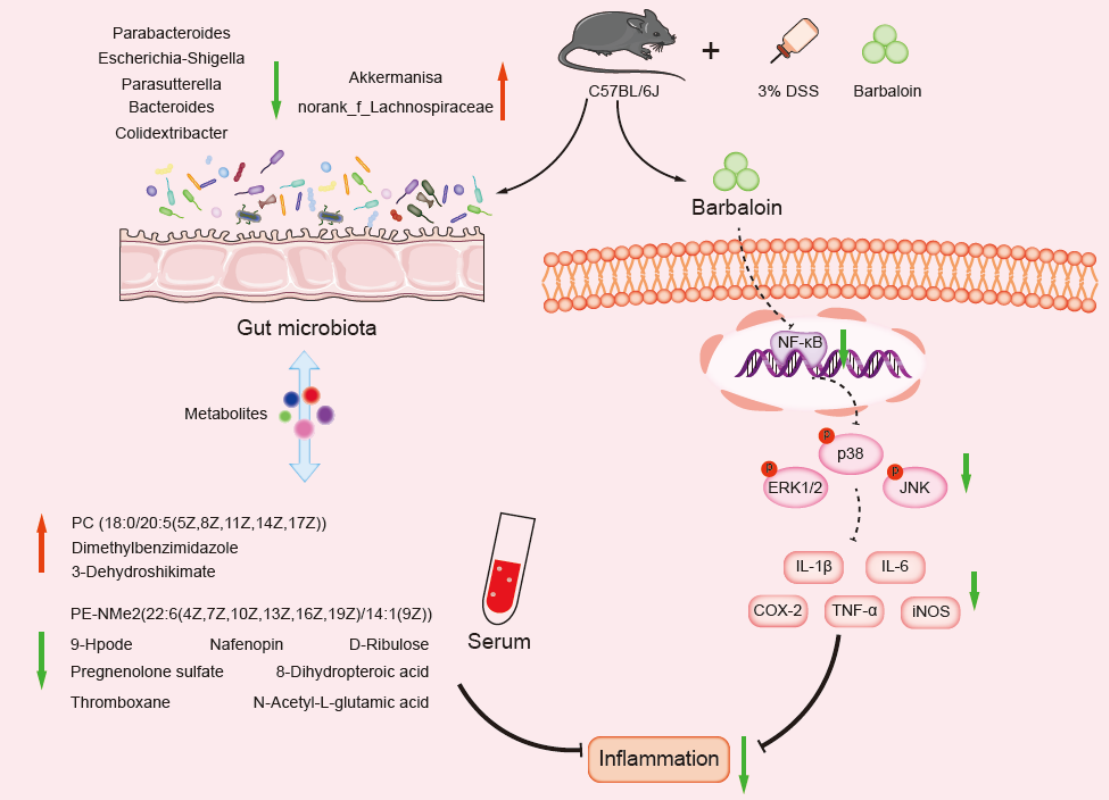


**Fig.13.** The potential anti-colitis mechanism of BAR.

## Data Availability Statement

All relevant data about this research can be requested from the corresponding author.

## Conflicts of Interest

The authors declare no conflict of interest.

## Acknowledgments

This research was financially supported by the Key Project of State Key R & D Program, China (No. 2022YFF1100200), the Postgraduate Scientific Research Innovation Project of Hunan Province (CX20240070).

## References

[1] M. Kishi, F. Hirai, N. Takatsu, et al. A review on the current status and definitions of activity indices in inflammatory bowel disease: how to use indices for precise evaluation. J. Gastroenterol. 57 (2022) 246-266. https://doi.org/10.1007/s00535-022-01862-y.

[2] J.P. Segal, J.F. LeBlanc, A.L. Hart, Ulcerative colitis: An update. Clin. Med. (Lond) 21 (2021) 135-139.https://doi.org/10.7861/clinmed.2021-0080.

[3] A. Kohyama, K. Watanabe, A. Sugita, et al. Ulcerative colitis-related severe enteritis: an infrequent but serious complication after colectomy. J. Gastroenterol. 56 (2021) 240-249. https://doi.org/10.1007/s00535-020-01742-3.

[4] A.H. Keshteli, K.L. Madsen, L.A. Dieleman, Diet in the pathogenesis and management of ulcerative colitis; A review of randomized controlled dietary interventions. Nutrients 11 (2019) 1498. https://doi.org/10.3390/nu11071498.

[5] M. Agrawal, E.A. Spencer, J.F. Colombel, et al., Approach to the management of recently diagnosed inflammatory bowel disease patients: A user's guide for adult and pediatric gastroenterologists. Gastroenterology 161 (2021) 47-65. https://doi.org/10.1053/j.gastro.2021.04.063.

[6] F. Magro, G. Cordeiro, A.M. Dias, et al., Inflammatory bowel disease-Non-biological treatment. Pharmacol. Res. 160 (2020) 105075. https://doi.org/10.1016/j.phrs.2020.105075.

[7] H.M. Cohn, M. Dave, E.V.Jr. Loftus, Understanding the cautions and contraindications of immunomodulator and biologic therapies for use in inflammatory bowel disease. Inflamm. Bowel. Dis. 23 (2017) 1301-1315. https://doi.org/10.1097/MIB.0000000000001199.

[8] J.S. Davis, D. Ferreira, E. Paige, et al., Infectious complications of biological and small molecule targeted immunomodulatory therapies. Clin. Microbiol. Rev. 33 (2020) e00035-19. https://doi.org/10.1128/CMR.00035-19.

[9] W. Zeng, D. He, Y. Xing, et al., Internal connections between dietary intake and gut microbiota homeostasis in disease progression of ulcerative colitis: A review. Food Sci. Hum. Wellness 10 (2021) 119-130. https://doi.org/10.1016/j.fshw.2021.02.016.

[10] D. Jonkers, J. Penders, A. Masclee, et al., Probiotics in the management of inflammatory bowel disease: A systematic review of intervention studies in adult patients. Drugs 72 (2012) 803-823. https://doi.org/10.2165/11632710-000000000-00000.

[11] Y. Gao, K.I. Kuok, Y. Jin, et al., Biomedical applications of Aloe vera. Crit. Rev. Food Sci. Nutr. 59 (2019) S244-S256. https://doi.org/10.1080/10408398.2018.1496320.

[12] Y. Li, J.G. Jiang, Health functions and structure-activity relationships of natural anthraquinones from plants. Food Funct. 9 (2018) 6063-6080. https://doi.org/10.1039/c8fo01569d.

[13] J.J. Yan, G.H. Du, X.M. Qin, et al., Baicalein attenuates the neuroinflammation in LPS-activated BV-2 microglial cells through suppression of pro-inflammatory cytokines, COX2/NF-κB expressions and regulation of metabolic abnormality. Int. Immunopharmacol. 79 (2020) 106092. https://doi.org/10.1016/j.intimp.2019.106092.

[14] W. Lee, S. Yang, C. Lee, et al., Aloin reduces inflammatory gene iNOS via inhibition activity and p-STAT-1 and NF-κB. Food Chem. Toxicol. 126 (2019) 67-71. https://doi.org/10.1016/j.fct.2019.02.025.

[15] L. Chen, H. Teng, Z. Jia, et al., Intracellular signaling pathways of inflammation modulated by dietary flavonoids: The most recent evidence. Crit. Rev. Food Sci. Nutr. 58 (2018) 2908-2924. https://doi.org/10.1080/10408398.2017.1345853.

[16] L. Gai, L. Chu, R. Xia, et al., Barbaloin attenuates mucosal damage in experimental models of rat colitis by regulating inflammation and the AMPK signaling pathway. Med. Sci. Monit. 25 (2019) 10045-10056. https://doi.org/doi:10.12659/MSM.918935.

[17] H. Jiang, G.F. Shi, Y.X. Fang, et al., Aloin A prevents ulcerative colitis in mice by enhancing the intestinal barrier function via suppressing the Notch signaling pathway. Phytomedicine 106 (2022) 154403.https://doi.org/10.1016/j.phymed.2022.154403.

[18] A.M. Valdes, J. Walter, E. Segal, et al., Role of the gut microbiota in nutrition and health. BMJ. 361 (2018) k2179. https://doi.org/10.1136/bmj.k2179.

[19] H.C. Wastyk, G.K. Fragiadakis, D. Perelman, et al., Gut-microbiota-targeted diets modulate human immune status. Cell 184 (2021) 4137-4153.https://doi.org/10.1016/j.cell.2021.06.019.

[20] A. Lavelle, H. Sokol, Gut microbiota-derived metabolites as key actors in inflammatory bowel disease. Nat. Rev. Gastroenterol. Hepatol. 17 (2020) 223-237. https://doi.org/10.1038/s41575-019-0258-z.

[21] C. Christensen, A. Knudsen, E.K. Arnesen, et al., Diet, food, and nutritional exposures and inflammatory bowel disease or progression of disease: An umbrella review. Adv. Nutr. 15 (2024) 100219. https://doi.org/10.1016/j.advnut.2024.100219.

[22] M.D. Boudreau, G.R. Olson, V.P. Tryndyak, et al., Aloin, a component of the aloe vera plant leaf, induces pathological changes and modulates the composition of microbiota in the large intestines of F344/N male rats. Toxicol. Sci. 158 (2017) 302-318. https://doi.org/10.1093/toxsci/kfx105

[23] J. Su, J. Xiao, X. Deng, et al., Combining aloin with TIENAM ameliorates cecal ligation and puncture-induced sepsis in mice by attenuating inflammation and modulating abdominal cavity microbiota. Int. Immunopharmacol. 141 (2024) 112925. https://doi.org/10.1016/j.intimp.2024.112925.

[24] Z. Chu, Z. Hu, F. Yang, et al., Didymin ameliorates dextran sulfate sodium (DSS)-induced ulcerative colitis by regulating gut microbiota and amino acid metabolism in mice. Metabolites 14 (2024) 547. https://doi.org/10.3390/metabo14100547.

[25] Z. Chu, L. Zeng, F. Yang, et al., Network pharmacology combined with molecular docking and molecular dynamic simulation to reveal the potential mechanism of lentinan ameliorating hyperlipidemia. Food Biosci. 60 (2024) 104306. https://doi.org/10.1016/j.fbio.2024.104306.

[26] N. Liu, Z. Yang, Y. Liu, et al., Identification of a putative SARS-CoV-2 main protease inhibitor through in silico screening of self-designed molecular library. Int. J. Mol. Sci. 24 (2023) 11390. https://doi.org/10.3390/ijms241411390.

[27] R. Majumder, C.K. Das, M. Mandal, Lead bioactive compounds of Aloe vera as potential anticancer agent. Pharmacol. Res. 148 (2019) 104416. https://doi.org/10.1016/j.phrs.2019.104416.

[28] J. Bai, B. Qian, T. Cai, et al., Aloin attenuates oxidative stress, inflammation, and CCl4-induced liver fibrosis in mice: possible role of tgf-β/smad signaling. J. Agric. Food Chem. 71 (2023) 19475-19487. https://doi.org/10.1021/acs.jafc.3c01721.

[29] W. Lee, G.S. Jeong, M.C. Baek, et al., Renal protective effects of aloin in a mouse model of sepsis. Food Chem. Toxicol. 132 (2019) 110651. https://doi.org/10.1016/j.fct.2019.110651.

[30] Y. Yang, J.J. Wu, J. Xia, et al., Can aloin develop to medicines or healthcare products? Biomed. Pharmacother. 153 (2022) 113421. https://doi.org/10.1016/j.biopha.2022.113421.

[31] S.M. Lewis, A. Williams, S.C. Eisenbarth, Structure and function of the immune system in the spleen. Sci. Immunol. 4 (2019) eaau6085. https://doi.org/10.1126/sciimmunol.aau6085.

[32] Z. Wang, S. Li, Y. Cao, et al., Oxidative stress and carbonyl lesions in ulcerative colitis and associated colorectal cancer. Oxid. Med. Cell Longev. 2016 (2016) 9875298. https://doi.org/10.1155/2016/9875298.

[33] A. Bhattacharyya, R. Chattopadhyay, S. Mitra, et al., Oxidative stress: An essential factor in the pathogenesis of gastrointestinal mucosal diseases. Physiol. Rev. 94 (2014) 329-354. https://doi.org/10.1152/physrev.00040.2012.

[34] C.L. Hawkins, M.J. Davies, Role of myeloperoxidase and oxidant formation in the extracellular environment in inflammation-induced tissue damage. Free Radic. Biol. Med. 172 (2021) 633-651. https://doi.org/10.1016/j.freeradbiomed.2021.07.007.

[35] T. Otani, M. Furuse, Tight junction structure and function revisited. Trends Cell Biol. 30 (2020) 805-817. https://doi.org/10.1016/j.tcb.2020.08.004.

[36] N. Benech, H. Sokol, Targeting the gut microbiota in inflammatory bowel diseases: where are we? Curr. Opin. Microbiol. 74 (2023) 102319. https://doi.org/10.1016/j.mib.2023.102319.

[37] L.W. Kaminsky, R. Al-Sadi, T.Y. Ma, IL-1β and the intestinal epithelial tight junction barrier. Front. Immunol. 12 (2021) 767456. https://doi.org/10.3389/fimmu.2021.767456.

[38] M.G. Rooks, W.S. Garrett, Gut microbiota, metabolites and host immunity. Nat. Rev. Immunol. 16 (2016) 341-352. https://doi.org/10.1038/nri.2016.42.

[39] S. Liu, W. Zhao, P. Lan, et al., The microbiome in inflammatory bowel diseases: from pathogenesis to therapy. Protein. Cell 12 (2021) 331-345.

[40] N.A. Nagalingam, S.V. Lynch, Role of the microbiota in inflammatory bowel diseases. Inflamm. Bowel. Dis. 18 (2012) 968-984. https://doi.org/10.1002/ibd.21866.

[41] Z. Hu, Z. Chu, X. Ling, Sinensetin from citrus peel alleviates DSS-induced inflammation by regulating gut microbiota and serum metabolism in mice. Food Biosci. 62 (2024) 105066. https://doi.org/10.1016/j.fbio.2024.105066.

[42] X. Xia, H. Lin, F. Luo, Oryzanol ameliorates DSS-Stimulated gut barrier damage via targeting the gut microbiota accompanied by the TLR4/NF-κB/NLRP3 cascade response in vivo. J. Agric. Food Chem. 70 (2022) 15747-15762. https://doi.org/10.1021/acs.jafc.2c04354.

[43] I. Koboziev, C. Reinoso Webb, K.L. Furr, et al., Role of the enteric microbiota in intestinal homeostasis and inflammation. Free Radic. Biol. Med. 68 (2014) 122-133. https://doi.org/10.1016/j.freeradbiomed.2013.11.008.

[44] S. Stojanov, A. Berlec, B. Štrukelj, The influence of probiotics on the Firmicutes/Bacteroidetes ratio in the treatment of obesity and inflammatory bowel disease. Microorganisms 8 (2020) 1715. https://doi.org/10.3390/microorganisms8111715.

[45] F.J. Osuna-Prieto, H. Xu, L. Ortiz-Alvarez, et al., The relative abundance of fecal bacterial species belonging to the Firmicutes and Bacteroidetes phyla is related to plasma levels of bile acids in young adults. Metabolomics. 19 (2023) 54. https://doi.org/10.1007/s11306-023-02016-8.

[46] J.J. Gilbreath, W.L. Cody, D.S. Merrell, Change is good: Variations in common biological mechanisms in the epsilonproteobacterial genera Campylobacter and Helicobacter. Microbiol. Mol. Biol. Rev. 75 (2011) 84-132. https://doi.org/10.1128/MMBR.00035-10.

[47] S. Zhu, M. Han, S. Liu, Composition and diverse differences of intestinal microbiota in ulcerative colitis patients. Front. Cell Infect. Microbiol. 12 (2022) 953962. https://doi.org/10.3389/fcimb.2022.953962.

[48] Z. Wang, J. Chen, Z. Chen, Clinical effects of ursodeoxycholic acid on patients with ulcerative colitis may improve via the regulation of IL-23-IL-17 axis and the changes of the proportion of intestinal microflora. Saudi. J. Gastroenterol. 27 (2021) 149-157. https://doi.org/10.4103/sjg.SJG_462_20.

[49] D. González, M. Morales-Olavarria, B. Vidal-Veuthey, et al., Insights into early evolutionary adaptations of the Akkermansia genus to the vertebrate gut. Front. Microbiol. 14 (2023) 1238580. https://doi.org/10.3389/fmicb.2023.1238580.

[50] C. Mo, X. Lou, J. Xue, et al., The influence of Akkermansia muciniphila on intestinal barrier function. Gut Pathog. 16 (2024) 41. https://doi.org/10.1186/s13099-024-00635-7.

[51] C.W. Ko, J. Qu, D.D. Black, et al., Regulation of intestinal lipid metabolism: current concepts and relevance to disease. Nat. Rev. Gastroenterol. Hepatol. 17 (2020) 169-183. https://doi.org/10.1038/s41575-019-0250-7.

[52] E.M. Corteselli, E. Gibbs-Flournoy, S.O. Simmons, Long chain lipid hydroperoxides increase the glutathione redox potential through glutathione peroxidase 4. Biochim. Biophys. Acta. Gen. Subj. 1863 (2019) 950-959. https://doi.org/10.1016/j.bbagen.2019.03.002.

[53] N.S. Yarla, A. Bishayee, G. Sethi, Targeting arachidonic acid pathway by natural products for cancer prevention and therapy. Semin. Cancer Biol. 40-41 (2016) 48-81. https://doi.org/10.1016/j.semcancer.2016.02.001.

[54] A. Sacco, A. Bruno, A. Contursi, Platelet-specific deletion of cyclooxygenase-1 ameliorates dextran sulfate sodium-induced colitis in mice. J. Pharmacol. Exp. Ther. 370 (2019) 416-426. https://doi.org/10.1124/jpet.119.259382.

[55] A. Parker, S. Fonseca, S.R. Carding, Gut microbes and metabolites as modulators of blood-brain barrier integrity and brain health. Gut Microbes. 11 (2020) 135-157. https://doi.org/10.1080/19490976.2019.1638722.

[56] W. Yang, Y. Cong, Gut microbiota-derived metabolites in the regulation of host immune responses and immune-related inflammatory diseases. Cell Mol. Immunol. 18 (2021) 866-877. https://doi.org/10.1038/s41423-021-00661-4.

[57] C.W. Ha, Y.Y. Lam, A.J. Holmes, Mechanistic links between gut microbial community dynamics, microbial functions and metabolic health. World J. Gastroenterol. 20 (2014) 16498-16517. https://doi.org/10.3748/wjg.v20.i44.16498.

[58] J. Leiba, R. Özbilgiç, L. Hernández, et al., Molecular actors of inflammation and their signaling pathways: mechanistic insights from zebrafish. Biology. (Basel). 12 (2023) 153. https://doi.org/10.3390/biology12020153.

[59] K.M. Sheu, Hoffmann, A. Functional hallmarks of healthy macrophage responses: Their regulatory basis and disease relevance. Annu. Rev. Immunol. 40 (2022) 295-321. https://doi.org/10.1146/annurev-immunol-101320-031555.

[60] G. Wang, Q. Zhan, H. Wu, Suppression of lipopolysaccharide-induced activation of RAW 264.7 macrophages by Se-methylseleno-l-cysteine. Int. Immunopharmacol. 89 (2020) 107040. https://doi.org/10.1016/j.intimp.2020.107040.

[61] G.J. Huang, C.H. Pan, F.C. Liu, Anti-inflammatory effects of ethanolic extract of Antrodia salmonea in the lipopolysaccharide-stimulated RAW246.7 macrophages and the λ-carrageenan-induced paw edema model. Food Chem. Toxicol. 50 (2012) 1485-1493. https://doi.org/10.1016/j.fct.2012.01.041.

[62] T. Guo, Q. Lin, X. Li, et al., Octacosanol attenuates inflammation in both RAW264.7 macrophages and a mouse model of colitis. J. Agric. Food Chem. 65 (2017) 3647-3658. https://doi.org/10.1021/acs.jafc.6b05465.

[63] J. Brägelmann, C. Lorenz, S. Borchmann, et al., MAPK-pathway inhibition mediates inflammatory reprogramming and sensitizes tumors to targeted activation of innate immunity sensor RIG-I. Nat. Commun. 12 (2021) 5505. https://doi.org/10.1038/s41467-021-25728-8.

[64] L. Camacho-Barquero, I. Villegas, J.M. Sánchez-Calvo, et al., Curcumin, a Curcuma longa constituent, acts on MAPK p38 pathway modulating COX-2 and iNOS expression in chronic experimental colitis. Int. Immunopharmacol. 7 (2007) 333-342. https://doi.org/10.1016/j.intimp.2006.11.006.

[65] P. Huang, J. Han, L. Hui, MAPK signaling in inflammation-associated cancer development. Protein Cell 1 (2010) 218-226. https://doi.org/10.1007/s13238-010-0019-9.

[66] G.L. Johnson, R. Lapadat, Mitogen-activated protein kinase pathways mediated by ERK, JNK, and p38 protein kinases. Science 298 (2002) 1911-1912. https://doi.org/10.1126/science.1072682.

[67] X. Li, L. Cai, H. Xu, et al., Somatostatin regulates NHE8 protein expression via the ERK1/2 MAPK pathway in DSS-induced colitis mice. Am. J. Physiol. Gastrointest. Liver Physiol. 311 (2016) G954-G963. https://doi.org/10.1152/ajpgi.00239.2016.

[68] D.Y. Fann, Y.A. Lim, Y.L. Cheng, et al., Evidence that NF-κB and MAPK signaling promotes NLRP inflammasome activation in neurons following ischemic stroke. Mol. Neurobiol. 55 (2018) 1082-1096. https://doi.org/10.1007/s12035-017-0394-9.

[69] J. Zhong, F. Wang, Z. Wang, et al., Aloin attenuates cognitive impairment and inflammation induced by d-galactose via down-regulating ERK, p38 and NF-κB signaling pathway. Int. Immunopharmacol. 72 (2019) 48-54. https://doi.org/10.1016/j.intimp.2019.03.050.